Article

Cell Reports

# SMUG1 Promotes Telomere Maintenance through Telomerase RNA Processing

## Graphical Abstract

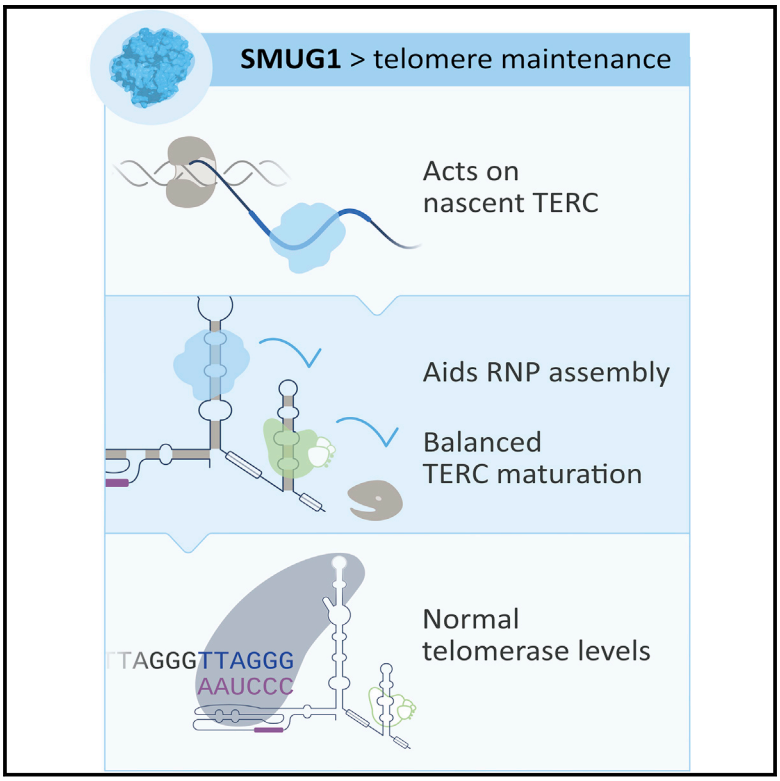


## Authors

Penelope Kroustallaki, Lisa Lirussi, Sergio Carracedo, ..., Pål Sætrom, Sarantis Gagos, Hilde Nilsen

## Correspondence

hilde.nilsen@medisin.uio.no

## In Brief

Kroustallaki et al. show that the single-strand-selective uracil-DNA glycosylase (SMUG1) functions in telomere maintenance, by removing modified bases from telomeric DNA and also by regulating modified bases in the telomerase RNA component (hTERC). SMUG1-knockout cells accumulate hTERC containing modified bases that interfere with binding of DKC1. Consequently, SMUG1-knockout cells and mice exhibit telomere maintenance defects.

## Highlights

- The SMUG1-DNA glycosylase promotes maturation of the telomeric DNA component, hTERC
- SMUG1 regulates the presence of base modifications in hTERC
- SMUG1 promotes DKC1 binding and stability of hTERC
- hTERC levels limit telomerase activity in human SMUG1-knockout cells

Kroustallaki et al., 2019, Cell Reports *28*, 1690–1702
August 13, 2019 
https://doi.org/10.1016/j.celrep.2019.07.040

CellPress

OPEN ACCESS
CellPress

Cell Reports
Article

# SMUG1 Promotes Telomere Maintenance through Telomerase RNA Processing

Penelope Kroustallaki,[1,2,8] Lisa Lirussi,[1,2,8] Sergio Carracedo,[1,2] Panpan You,[1,2] Q. Ying Esbensen,[1,2] Alexandra Götz,[1,2] Laure Jobert,[1,9] Lene Alsøe,[1,2] Pål Sætrom,[3,4,5,6] Sarantis Gagos,[7] and Hilde Nilsen[1,2,10,*]

[1]Department of Clinical Molecular Biology, University of Oslo, 0318 Oslo, Norway
[2]Department of Clinical Molecular Biology (EpiGen), Akershus University Hospital, 1478 Lørenskog, Norway
[3]Department of Clinical and Molecular Medicine, Norwegian University of Science and Technology, NTNU, 7491 Trondheim, Norway
[4]Department of Computer Science, Norwegian University of Science and Technology, NTNU, 7491 Trondheim, Norway
[5]Bioinformatics Core Facility-BioCore, Norwegian University of Science and Technology, NTNU, 7491 Trondheim, Norway
[6]K.G. Jebsen Center for Genetic Epidemiology, Norwegian University of Science and Technology, NTNU, 7491 Trondheim, Norway
[7]Center of Clinical, Experimental Surgery & Translational Research, Biomedical Research Foundation, Academy of Athens, Athens, Greece
[8]These authors contributed equally
[9]Present address: LifeTechnologies AS, Ullernschauseen 52, 0379 Oslo, Norway
[10]Lead Contact
*Correspondence: hilde.nilsen@medisin.uio.no
https://doi.org/10.1016/j.celrep.2019.07.040

## SUMMARY

**Telomerase biogenesis is a complex process where several steps remain poorly understood. Single-strand-selective uracil-DNA glycosylase (SMUG1) associates with the DKC1-containing H/ACA ribonucleoprotein complex, which is essential for telomerase biogenesis. Herein, we show that SMUG1 interacts with the telomeric RNA component (*hTERC*) and is required for co-transcriptional processing of the nascent transcript into mature *hTERC*. We demonstrate that SMUG1 regulates the presence of base modifications in *hTERC*, in a region between the CR4/CR5 domain and the H box. Increased levels of *hTERC* base modifications are accompanied by reduced DKC1 binding. Loss of SMUG1 leads to an imbalance between mature *hTERC* and its processing intermediates, leading to the accumulation of 3′-polyadenylated and 3′-extended intermediates that are degraded in an EXOSC10-independent RNA degradation pathway. Consequently, SMUG1-deprived cells exhibit telomerase deficiency, leading to impaired bone marrow proliferation in *Smug1*-knockout mice.**

## INTRODUCTION

Telomerase is a specialized ribonucleoprotein (RNP) complex that extends telomeric repeats at the ends of chromosomes (de Lange, 2005; Morin, 1989). The telomerase holoenzyme consists of three main subunits: the telomerase reverse transcriptase (hTERT), the telomerase RNA component (*hTERC*), and the dyskerin complex (DKC1, NHP2, NOP1, and GAR1) (Egan and Collins, 2012; Schmidt and Cech, 2015). *hTERC* is a highly structured non-coding RNA that carries the complementary template of the telomeric repeat sequence and two H/ACA domains that bind to dyskerin (Egan and Collins, 2012). The *hTERC*/dyskerin RNP complex and hTERT associate in both nucleoli and Cajal bodies (CBs) during S phase, suggesting that both these subnuclear structures are involved in the biogenesis and trafficking of the telomerase complex (Lee et al., 2014; MacNeil et al., 2016). *hTERC* biogenesis is a multistep process. First, *hTERC* is transcribed by RNA polymerase II (Pol II) to a primary transcript that can extend several hundred nucleotides downstream of the *hTERC* gene body (Nguyen et al., 2015; Tseng et al., 2015). The H/ACA complex is co-transcriptionally assembled and may mediate *hTERC* transcriptional termination and, thus, determine the length of the 3′ extension (MacNeil et al., 2016). Subsequent end-processing steps, leading to the formation of the 451-nt-long mature *hTERC*, involve polyadenylation by the Trf4/5-Air1/2-(TRAMP) complex, or the PARN/PABPN1 machinery, and processing by the nuclear exosome-targeting (NEXT) complex (Nguyen et al., 2015; Tseng et al., 2015). The balance between maturation and exosomal degradation determines the level of mature *hTERC* (MacNeil et al., 2016; Zinder and Lima, 2017). Other RNA degradation pathways might also be involved in the removal of *hTERC* intermediates (Schmidt and Cech, 2015; Zinder and Lima, 2017), and the detailed molecular mechanisms of *hTERC* maturation are not fully understood.

We recently demonstrated that the single-strand-selective uracil (SMUG1)-DNA glycosylase interacts and co-localizes with the pseudouridine synthase DKC1 (Jobert et al., 2013). DKC1 is involved in the biogenesis and maturation of several RNA classes, such as rRNA (Ge et al., 2010). SMUG1 associates with the 47S rRNA precursor, which is a major substrate of DKC1, and loss of SMUG1 leads to rRNA processing defects and accumulation of 5-hydroxymethyluridine (hmU) in rRNA. Thus, in addition to its function in DNA base excision repair (BER), SMUG1 acts in rRNA quality control (Jobert et al., 2013).

As DKC1 functions both to support telomerase biogenesis in nucleoli and CBs as a structural component of the telomerase holoenzyme (Mitchell et al., 1999; Venteicher et al., 2009; Lee et al., 2014), we tested a possible role for SMUG1 in telomere maintenance. We show that SMUG1 is present in CBs and observed a

significant decrease in telomere length in human SMUG1-knockout (KO) cells due to insufficient levels of mature *hTERC* to support telomerase activity. *hTERC* accumulated base modifications between the CR4/CR5 domain and the H box, a region important for DKC1 binding. Consistently, DCK1 was bound less efficiently in SMUG1-KO cells, leading to *hTERC* degradation. We conclude that SMUG1 promotes *hTERC* stability by regulating the presence of modified bases to allow binding of DKC1.

## RESULTS

### SMUG1 Influences DKC1 Localization

We previously observed that overexpression of a SMUG1 mutant unable to interact with DKC1 (E29R/E33R) affected DKC1 localization in HeLa cells (Jobert et al., 2013). To confirm that disruption of the SMUG1/DKC1 interaction surface perturbs proper localization of DKC1, we repeated these experiments in *Smug1*$^{-/-}$ mouse embryonic fibroblasts (MEFs) (Alsøe et al., 2017). To exclude any bias originating from possible small differences in cell-cycle distribution, we scored the ring-shaped structures formed by DKC1 (DKC1 circles) during S phase (Lee et al., 2014). In *Smug1*$^{-/-}$ MEFs we observed fewer DKC1 circles (white arrows) and the appearance of dense nucleolar bodies (yellow arrows) (Figures 1A and 1B). The number of DKC1 circles could not be fully restored in cells stably expressing neither wild-type SMUG1 nor a mutant that does not have DNA-glycosylase activity on RNA substrates (H241L) (Figures 1A, 1B, and S1A). Confirming our previous data, expression of the DKC1-binding mutant exacerbated the phenotype (Figures 1A and 1B). SMUG1/DKC1 interaction affects the DKC1 distribution pattern in nucleoli, which has been suggested to be the site for the biogenesis of the telomerase holoenzyme (Lee et al., 2014) before transport to the CBs (MacNeil et al., 2016). Interestingly, *in situ* proximity ligation assay (PLA) showed SMUG1-Coilin interaction in the nucleus and CBs (Figures 1C and S1B). Taken together, SMUG1 influences DKC1 organization in the nucleoli, possibly suggesting a role of SMUG1 in telomerase biogenesis.

### *Smug1*$^{-/-}$ Mice Exhibit Telomere Maintenance Defects

As DKC1 is essential for telomerase biogenesis and regulation of telomere length (Mitchell et al., 1999), we asked whether SMUG1 functions in telomere maintenance. Telomere chromatin immunoprecipitation (TeloChIP) showed that SMUG1 associated with telomeric chromatin (Figure 2A). SMUG1 could not be detected at telomeres by telomere-specific fluorescent *in situ* hybridization (FISH) (Figure S1C), suggesting that SMUG1 transiently associates with telomeric DNA, consistent with the BER function. In tissue harvested from 3- to 4-month-old *Smug1*$^{-/-}$ mice, a significantly reduced average telomere length was found in the heart (62% reduction; $p = 0.017$) but not in the spleen and brain (Figure 2B). To assess whether accumulation of DNA base damage in the form of SMUG1 substrates occurred in telomeric DNA, we digested the genomic DNA with SMUG1 and APE1 prior to telomere length measurements by qPCR. The presence of damaged bases would be expected to reduce the amplification efficiency. In this assay, increased telomeric DNA damage was detected only in heart tissue (Figure 2B). The average telomere length was similar in *Smug1*$^{-/-}$ and isogenic wild-type MEFs (Figure 2C), but telomere-specific FISH revealed high frequencies of fragile telomeres in primary (Figures 2D and 2E) and transformed *Smug1*$^{-/-}$ MEFs (Figure S1D). Strand-specific telomere-FISH probes showed a doubling of fragile telomeres on the leading C-rich strand in primary MEFs (Figure 2E), while the G-rich strand was largely unaffected (Figure S1E). Transformed MEFs had significantly more fragile telomeric signals in both strands (Figure S1D).

The fragile telomere phenotype was even more pronounced in *Smug1*$^{-/-}$ primary bone marrow cells. Both strands showed an increase in fragile telomeres, but the increase was more pronounced on the C-rich strand where close to 4% of the telomeric signals showed fragility on the C-strand, compared to less than 1% in wild-type bone marrow cells (Figure 2F). To assess whether telomere fragility had functional relevance *in vivo*, we measured the colony-forming capacity of primary bone marrow explant cultures (Figure 2G). The colony-forming unit abilities of the erythrocyte (BFU-E) and granulocyte (CFU-G) lineages in *Smug1*$^{-/-}$ bone marrow explant cultures were reduced by 43% and 41%, respectively, in mice born from heterozygous parents (F1). As expected, based on a telomere maintenance phenotype, the colony-forming ability was further reduced in mice born from parents generated through five generations of interbreeding of homozygous *Smug1*-knockout mice (F6). In the F6 generation, the proliferative potentials of the macrophage lineage (CFU-M) and BFU-E were reduced by 40% and 61%, respectively (Figure 2G). Thus, loss of SMUG1 expression in mice led to reduced average telomere length and accumulation of telomere DNA damage in certain tissues. In addition, there was an asymmetric fragile-telomere phenotype affecting, primarily, the C-rich strand and reduced proliferative potential of primary bone marrow cells.

### Dramatic Telomere Attrition in SMUG1-KO Human Cells Is Independent of BER Function

As telomere-associated phenotypes might be masked by the long telomeres of mice, we procured a human cell line in which SMUG1 expression was abrogated by a two-nucleotide deletion that introduces a premature stop codon after Asn56 of SMUG1 (Figure 3A). As expected, *SMUG1* transcription was unaffected (Figure 3B), but no SMUG1 protein could be detected using an antibody directed toward an N-terminal epitope (Figure 3C). Thus, the mutation generated a loss-of-function, or extremely hypomorphic, allele. TeloChIP analysis revealed 4-fold enrichment of telomeric DNA in HAP1 SMUG1 wild-type (WT) cells relative to SMUG1-KO cells (Figure 3D), showing that SMUG1 also associates with telomeres in human cells.

Telomeric-FISH signals were barely detectable in SMUG1-KO cells, in stark contrast to the bright signals observed in the parental cell line (Figure 3E). Scoring of fragile telomeres was therefore not possible, but the fraction of telomeric signal-free ends was increased by at least 2-fold in two independent SMUG-KO clones (Figures 3E and S2A). The dramatic telomere attrition was confirmed by telomere restriction fragment (TRF) analysis, which showed that SMUG1-KO telomeres were 2.6 kb long on average, compared to 16.6 kb in isogenic WT cells (Figure 3F). The weak signals detected in lanes loaded with genomic DNA isolated from SMUG1-KO cells, despite equal loading, were also consistent with a reduced fraction of

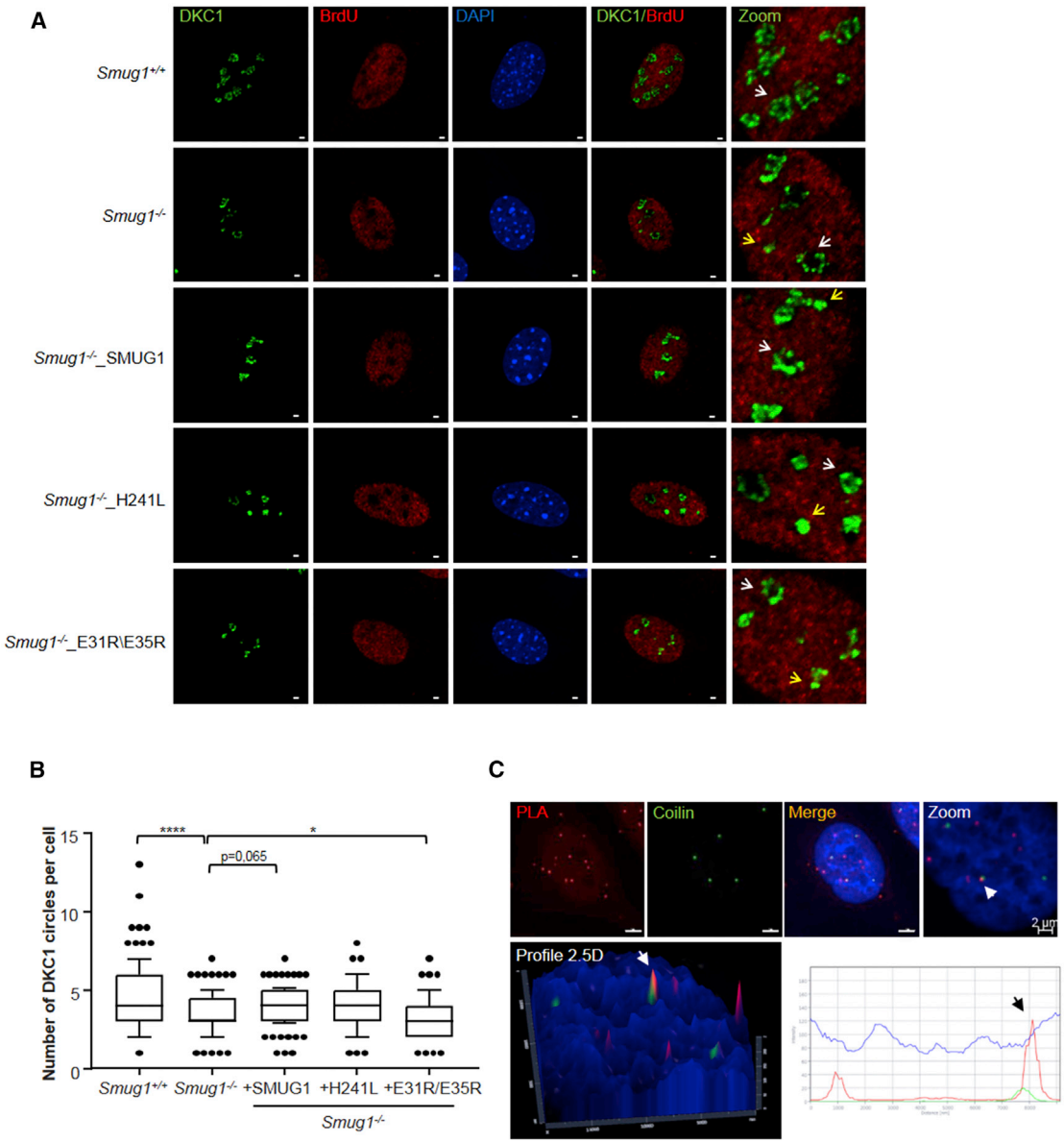


**Figure 1. SMUG1 Loss Leads to DKC1 Mislocalization**

(A) Localization of DKC1 in *Smug1*$^{+/+}$, *Smug1*$^{-/-}$, and *Smug1*$^{-/-}$ MEFs complemented with wild-type mouse SMUG1, or SMUG1 mutants that do not bind DNA (H241L) or DKC1 (E31R/E35R). Representative immunofluorescence (IF) images of BrdU (red) and DKC1 (green) staining are shown. DNA was labeled with 4′,6-diamidino-2-phenylindole (DAPI; blue). White and yellow arrows indicate DKC1 circles and dense bodies, respectively (scale bars, 2 μm).

(B) Boxplot showing the frequency of ring-shaped structures characteristic for DKC1 in S-phase cells, with whiskers representing the 10th and 90th percentiles; the dark line within the box represents the median. n = 100 cells, *p ≤ 0.05, and ****p ≤ 0.0001 (two-tailed Student's t test).

(C) Proximity ligation assay (PLA) showing FLAG-tagged SMUG1-Coilin interaction (red) in Cajal bodies (arrows). CBs were stained with Coilin (green). Scale bars, 1 μm.

telomeric DNA. To assess whether accumulation of DNA base damage in the form of SMUG1 substrates occurred in telomeric DNA, we added SMUG1 and APE1 to the restriction enzyme cocktail. Base damage present within the telomere restriction fragment would be expected to reduce fragment length. Indeed, the mean telomere length was further reduced in the SMUG1-KO cells (Figure 3F), whereas no change in telomere length was seen in WT cells. Thus, base damage was present in telomeres in the absence of SMUG1, reducing the average fragment length from 2.6 to 1.7 kb (Figure 3F, right).

The dramatic telomere attrition also affected the telomeric association of shelterin proteins. Both TRF1 and TRF2, which bind double-stranded telomeric DNA, exhibited a diffuse staining pattern in SMUG1-KO cells, in addition to the characteristic punctate telomere-specific staining (Figures 3G and S2B). The reduced binding of shelterin components was corroborated by

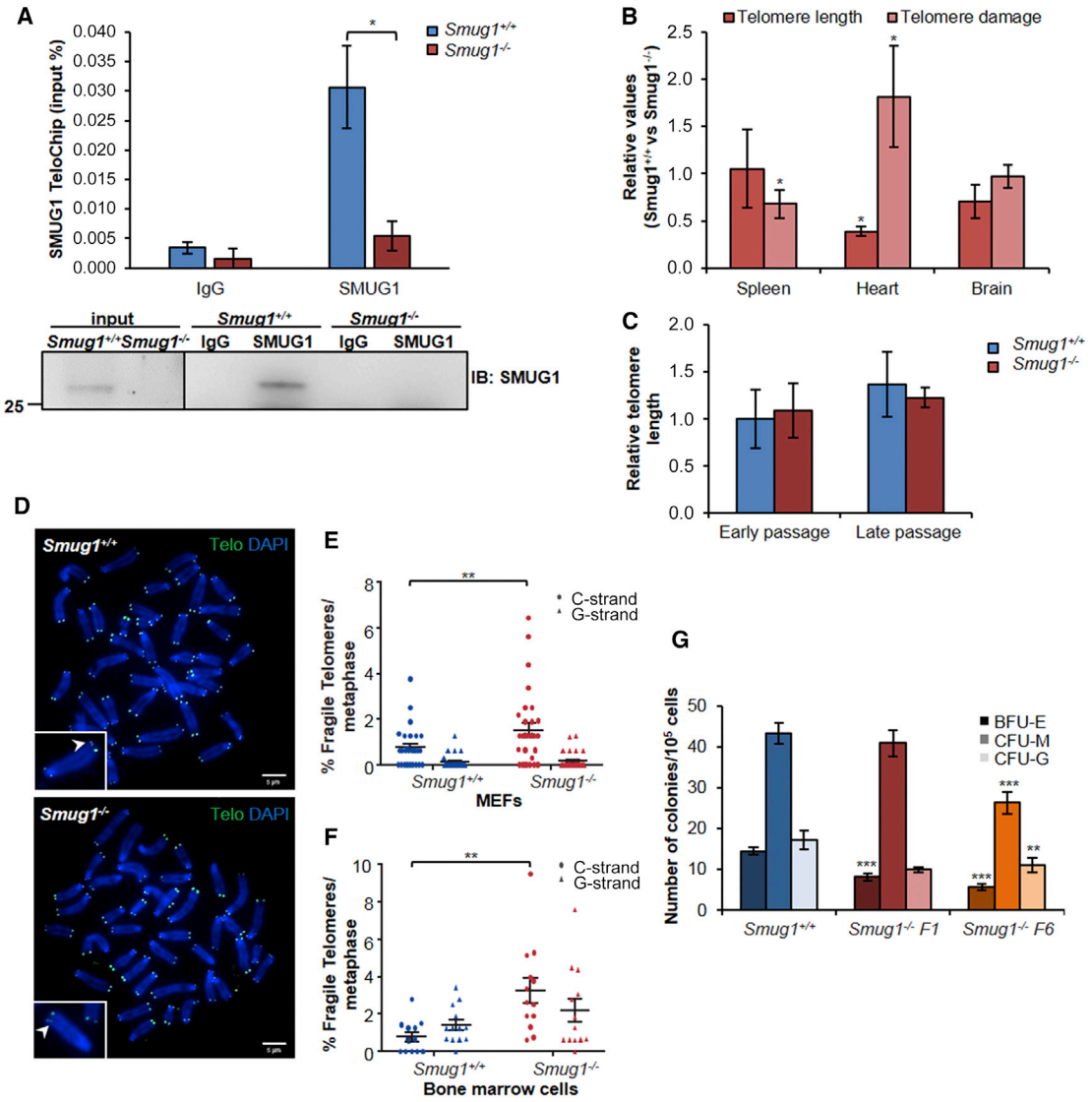


**Figure 2. *Smug1*$^{-/-}$ Mice Exhibit Telomere Maintenance Defects**

(A) TeloChIP followed by qPCR showing SMUG1 binding to telomere repeats in three independent MEF clones (top). Representative western blot of immunoprecipitation with IgG and SMUG1 antibodies (bottom).

(B) Telomere length and damage quantified in *Smug1*$^{-/-}$ mouse tissues (heart, spleen, and brain) by qPCR. Data are presented as fold change relative to wild-type mice.

(C) Telomere length in *Smug1*$^{+/+}$ and *Smug1*$^{-/-}$ MEF cells at early (0–10) and late (30–40) passages measured by qPCR.

(D) Peptide nucleic acid (PNA)-FISH in MEFs metaphases. Telomeres were hybridized with a telomere-specific probe (Telo, fluorescein isothiocyanate [FITC]) and chromosomes were stained with DAPI.

(E and F) Quantification of fragile telomere ends (FTEs) in primary MEFs (E) and in primary mouse bone marrow cells (circles represent C-strand; triangles represent G-strand) (F).

(G) Colony-forming capacity toward erythrocyte (BFU-E), granulocyte (CFU-G) and macrophage (CFU-M) lineages in bone marrow from *Smug1*$^{+/+}$ and *Smug1*$^{-/-}$ mice.

(A–C and G) Data represent mean ± SEM, n = 3. (E and F) Data represent mean ± SEM. (E) 30 and (F) 15 metaphases were scored. (A–C and E–G) *p $\leq$ 0.05, **p $\leq$ 0.01, and ***p $\leq$ 0.001 (two-tailed Student's t test).

the reduced association of POT1 and TFR2 with SMUG1-KO telomeres, as measured by TeloChIP (Figures 3H and 3I). We did not observe co-localization of TRF1 and the telomeric C-strand probe with γH2AX, suggesting that although shorter, SMUG1-KO telomeres remained bound to and protected by shelterin (Figures S2C and S2D). In conclusion, the loss of SMUG1 results in telomere maintenance defects characterized by fragile telomeres and tissue-specific telomere erosion in mice as well as dramatic telomere attrition in human HAP1 cells.

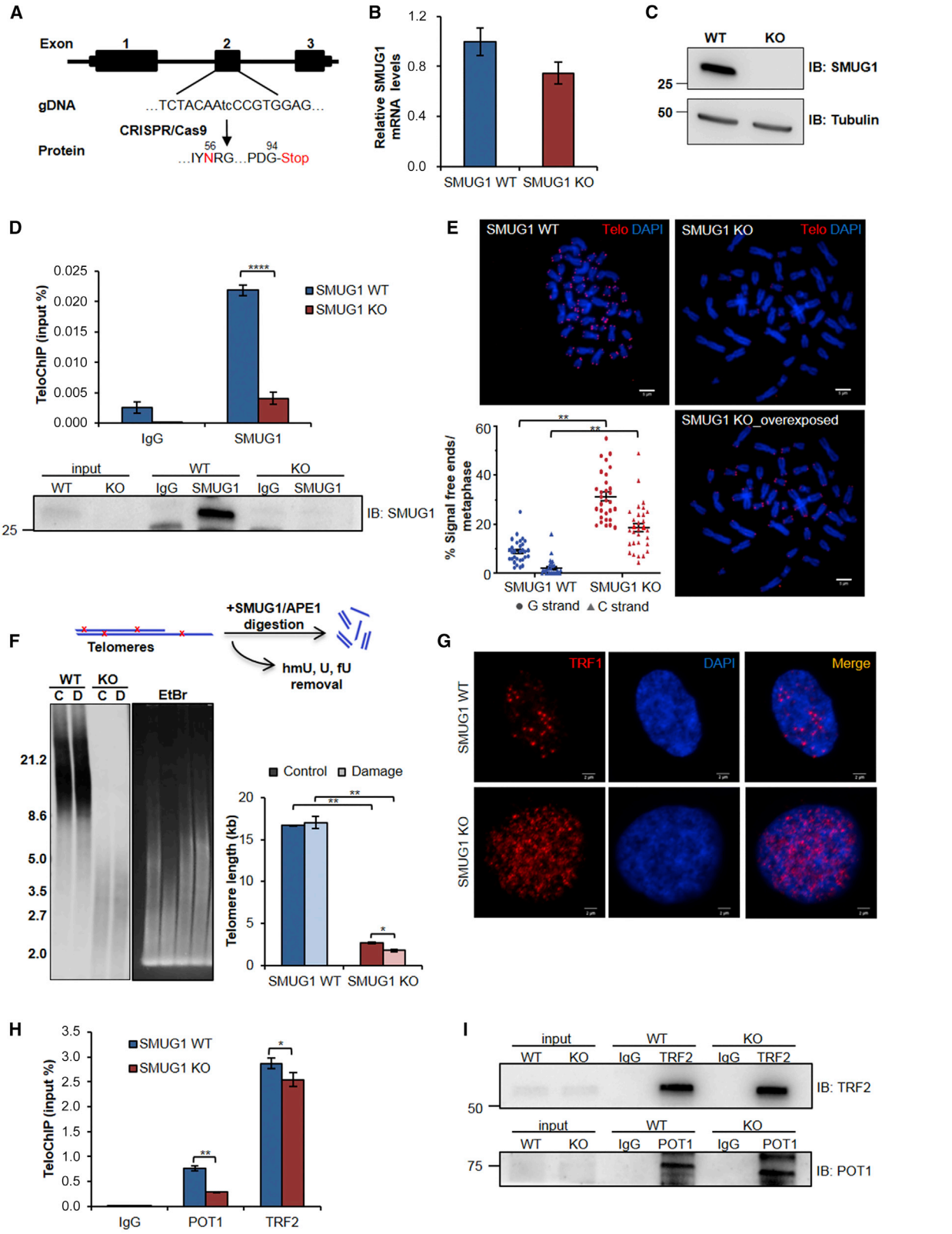


*(legend on next page)*

### Low *hTERC* Levels Limit Telomerase Activity in SMUG1-KO Human Cells

Prompted by the above telomeric phenotypes, we measured telomerase activity and found that SMUG1-KO cells displayed an 11-fold reduction of activity compared to the control cell line (Figure 4A). Although *hTERT* mRNA expression was somewhat higher in SMUG1-KO cells than in the control (Figure 4B), the amount of hTERT protein was unchanged (Figure 4C). In contrast, *hTERC* levels were 6-fold lower in SMUG1-KO cells than in WT cells as measured by qPCR (Figure 4B), northern blotting (Figure 4D), or RNA sequencing (RNA-seq) (Figures 4E, S3A, and S3B). Interestingly, the number of *hTERC* reads aligning downstream of the core pseudoknot domain was reduced (Figure 4E). Next, we tested whether *hTERC* levels were limiting for telomerase activity in SMUG1-KO cells by overexpressing *hTERC* or hTERT (Figures 4F and S3C). Indeed, transient expression of *hTERC* doubled telomerase activity in SMUG1-KO cells, whereas overexpressing hTERT had no effect (Figures 4F and S3C).

Similarly, *hTERC* levels and telomerase activity increased when SMUG1-WT expression was restored in two independent stable clones of SMUG1-KO cells (Figures 4G and S3D). Consistently, telomere length was also increased (Figure 4H). Overexpression of a SMUG1 mutant unable to bind nucleic acids (NABm) extended telomeres to some degree whereas overexpression of DKC1-binding mutant (DBm) mirrored SMUG1-KO cells (Figures S4D–S4F). In sum, this strongly suggests that telomere attrition in the absence of SMUG1 was caused by low telomerase activity, which was, in turn, a direct consequence of an *hTERC*-biogenesis defect in SMUG1-KO cells.

### SMUG1 Is Required for Co-transcriptional Processing of *hTERC*

Since the telomerase RNA component was found to be the limiting factor for telomerase activity in SMUG1-KO cells, we next asked whether SMUG1 binds *hTERC*. In RNA-immunoprecipitation experiments (RNA-IP), we detected 20-fold enrichment of *hTERC* using an anti-SMUG1 antibody compared to the immunoglobulin G (IgG) control (Figure 5A). Similarly, SMUG1 pull-down assays using recombinant SMUG1 protein as bait confirmed that SMUG1 bound directly *hTERC* without any intermediate protein when the total RNA isolated from HAP1 cells was used as prey (Figure S4A). The presence of modified bases in *hTERC* was essential for the interaction, as shown by the inability of SMUG1 to pull-down *in vitro* transcribed *hTERC* (Figures 5B and S4B). Mature *hTERC* levels are determined by the balance between processing and degradation (Figure S4C) (MacNeil et al., 2016). To test whether SMUG1 affects the equilibrium between different *hTERC* products, we measured the levels of the 451-nt mature *hTERC* and the two processing intermediates: 3′-extended and poly(A)-*hTERC* (Figure 5C). In SMUG1-KO cells, the reduced level of mature *hTERC* was accompanied by a 2.5-fold increase in 3′-extended *hTERC* (Figures 5C and 5D) and a 1.5-fold increase in polyadenylated intermediates (Figure 5C). Thus, the absence of SMUG1 disturbed the balance between mature *hTERC* and its processing intermediates.

To further characterize these processing intermediates, we performed 3′-rapid amplification of cDNA ends (RACE)-seq experiments, which showed that the majority of reads aligning to the *hTERC* gene terminated at the expected end, although there was a small increase in fragments aligning from positions 451 to 458 (Figure 5E). Long 3′-extended RNA polymerase II read-through products were not observed, suggesting that transcriptional termination and 3′ end processing are functional in SMUG1-KO cells. However, accumulation of 3′-extended *hTERC* with short tails (> 10 nt) was detected (Figures 5F and 5G). No dramatic differences in the poly(A) distribution could be observed (Figure 5F), but SMUG1-KO cells exhibited a 1.6-times-higher fraction of long (> 3 nt) poly(A) tails than WT cells (Figures 5G and 5H). Taken together, these data suggest that SMUG1-KO cells have mild *hTERC* processing defects but that the polyadenylation and main *hTERC* end-processing machinery are functional.

The low levels of *hTERC* in SMUG1-KO cells were not due to reduced transcription, as Pol II occupancy at two sites in the *hTERC* promoter (Aalbers et al., 2012; Zhao et al., 1998) and in the coding region was unchanged (Figures 5I, 5J, and S3F). Measurements of nascent *hTERC* kinetics also confirmed a similar transcription rate in HAP1 cells (Figure 5K). Moreover, ChIP experiments showed that SMUG1 was present together with Pol II at the *hTERC* promoter and gene body (Figure 5I). In contrast to Pol II, which was stabilized at the *hTERC* gene (Figure 5I, top), SMUG1 dissociated from chromatin after treatment with actinomycin D (ActD), suggesting that SMUG1 associates with

**Figure 3. Dramatic Telomere Attrition in SMUG1-KO Human Cells Is Independent of BER Function**

(A–C) Characterization of human HAP1 SMUG1-KO cells.

(A) Schematic representation of the 2-nt deletion, generating an early stop codon of the *SMUG1* gene.

(B and C) *SMUG1* mRNA levels quantified by qPCR (B) and western blot detection of the indicated proteins in HAP1 cells (C). Tubulin was used as loading control.

(D) TeloChIP followed by qPCR showing SMUG1 binding to telomere repeats (top). Enrichment of telomere sequences immunoprecipitated with the SMUG1 antibody is presented as percent of input DNA. Representative blot of immunoprecipitation with IgG and SMUG1 antibodies (bottom). IgG, negative control.

(E) PNA-FISH in metaphase spreads of HAP1 cells. Telomeres were hybridized with a telomere-specific probe (Telo, 5-Carboxytetramethylrhodamine [TAMRA]) and chromosomes were stained with DAPI. Quantification of signal-free ends is shown in the bottom left (circles represent G-strand; triangles represent C-strand).

(F) Representative southern blot of telomere restriction fragment length (TRF) assay in HAP1 cells is shown. Genomic DNA was digested with RsaI and HinfI restriction enzymes alone (Control, C) or RsaI and HinfI followed by incubation with SMUG1 and APE1 enzymes (DNA damage, D). Quantification of absolute telomere length (kb) is shown (right). Ethidium bromide staining is shown as loading control (left). An overview of the modified protocol is shown at the top.

(G) Representative IFs for TRF1 in HAP1 SMUG1-WT and SMUG1-KO cells (scale bars, 2 μm).

(H) POT1 and TRF2 binding to telomeric DNA in HAP1 cells assessed by TeloChIP followed by qPCR detection. Enrichment of the telomere-specific sequences immunoprecipitated with the indicated antibodies are presented as percent of input DNA. IgG, negative control.

(I) Representative blots of immunoprecipitation for IgG, TRF2, and POT1 antibodies.

(B, D, E, and H) Data represent mean ± SD, n = 3. (F) Data represent mean ± SD, n = 2. (E) 30 metaphases were scored. (D–F and H) *$p \leq 0.05$, **$p \leq 0.01$, and ****$p \leq 0.0001$ (two-tailed Student's t test).

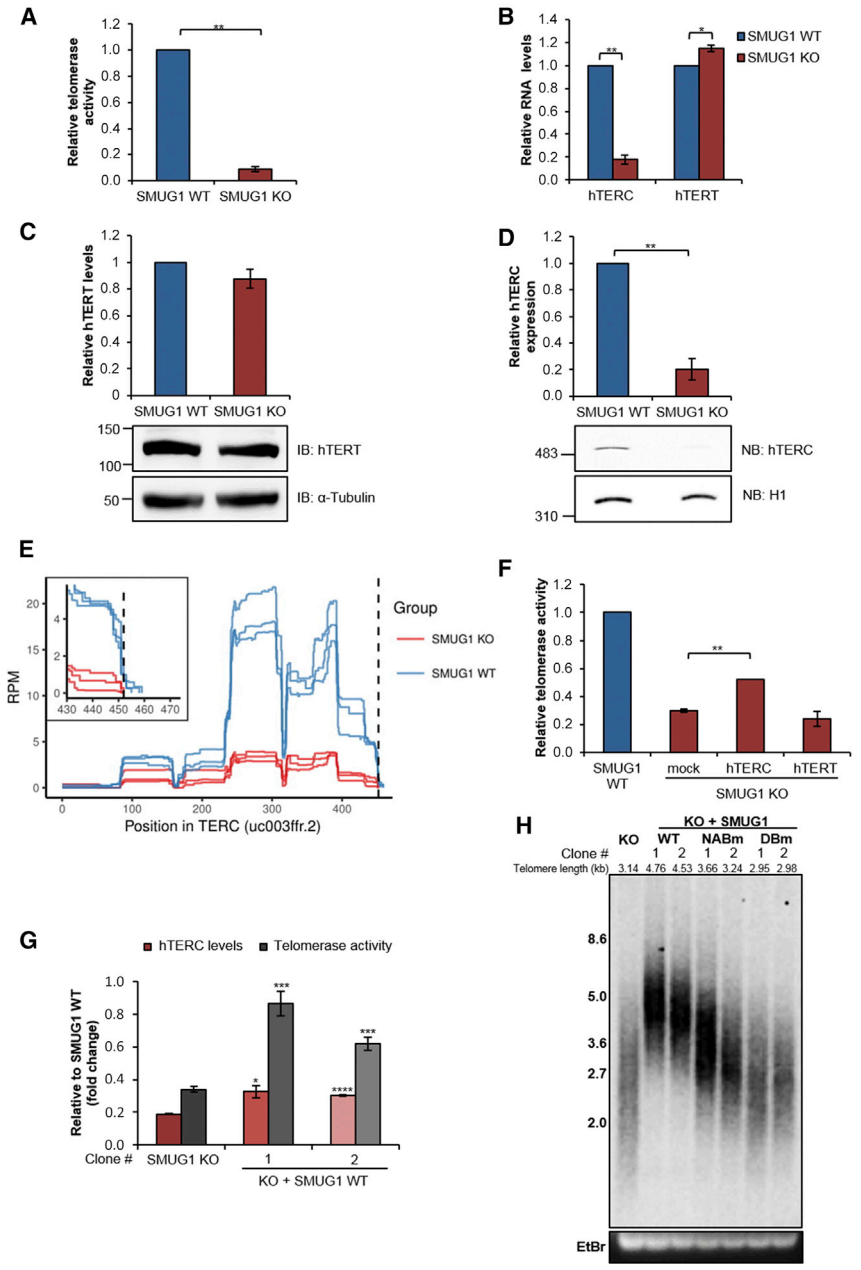


**Figure 4. Low *hTERC* Levels Limit Telomerase Activity in SMUG1-KO Human Cells**

(A) Telomerase activity of HAP1 cells quantified by qPCR.

(B) Relative RNA levels for *hTERC* and *hTERT* measured by qPCR.

(C) Representative western blot (WB) for hTERT (bottom) with quantification (top). Tubulin was used as loading control.

(D) Representative northern blot (NB) for *hTERC* (bottom) with quantification (top). *Histone H1* was used as loading control.

(E) Position-specific expression profiles for *hTERC*. The graphs show the normalized read depth within the *hTERC* gene locus. The vertical dashed line shows the canonical *hTERC* 3′ end as described by Moon et al. (2015); the insert shows a zoom-in of this 3′ end region.

(F) Telomerase activity quantified by droplet digital PCR (ddPCR) in HAP1 cells transfected with the indicated plasmids.

(G) Quantification of *hTERC* levels and telomerase activity measured via qPCR and ddPCR, respectively, in two SMUG1-KO clones stably expressing SMUG1 WT protein.

(H) Southern blot of the TRF assay in SMUG1-KO clones stably re-expressing WT and mutated SMUG1 unable to bind nucleic acids (NABm) and SMUG1 unable to bind DKC1 (DBm) is shown.

(A–D and G) Data represent means ± SD, n = 3. (F) Data represent means ± SD, n = 2. (A–D, F, and G) *p ≤ 0.05, **p ≤ 0.01, ***p ≤ 0.001, and ****p ≤ 0.0001 (two-tailed Student's t test).

## SMUG1 Is Required for *hTERC* Maturation

Binding of SMUG1 to *hTERC* in RNA isolated from cells but not to *in vitro* transcribed *hTERC* strongly suggested that binding requires the presence of modified bases (Figure 5B). Thus, we asked if SMUG1 is required to remove modified or damaged *hTERC* molecules. Since the *hTERC* levels in SMUG1-KO cells were too low to allow direct detection of RNA damage by liquid chromatography-tandem mass spectrometry (LC-MS/MS) (Jobert et al., 2013), we established an assay that detected the presence of SMUG1 substrates in specific regions of the *hTERC* transcript. The assay was based on reduced amplification of transcripts that contained modified bases after incubation with SMUG1 (Figure 6A, left). Interestingly, there was no reduction of amplification efficiency upon enzyme treatment using primers that recognized the 5′ end of the *hTERC* transcript (Figure 6A, right). However, when using primers that amplified a fragment between the *hTERC* CR4/CR5 domain and the H box, we observed reduced amplification of RNA isolated from SMUG1-KO cells. The drop in amplification efficiency corresponded to a 20-fold increase in SMUG1-induced fragmentation at the *hTERC* 3′ region in RNA isolated from

the actively transcribing Pol II complex (Figure 5I, bottom). Interestingly, stabilization of Pol II at the *hTERC* gene after ActD treatment was not seen in SMUG1-KO cells (Figure 5I), suggesting that SMUG1 promotes stability of the stalled Pol II complex. Click-iT experiments showed an increased initial decay rate of *hTERC* in SMUG1-KO cells at 4 h that appeared to stabilize after 24 h (Figure 5L). No differences in *hTERC* transcription could be detected (Figures 5I and 5K), indicating that post-transcriptional mechanisms are the main cause of the observed instability of *hTERC* in SMUG1-KO cells. Taken together, our data show that SMUG1 is required for co-transcriptional processing of *hTERC* and affects its decay.

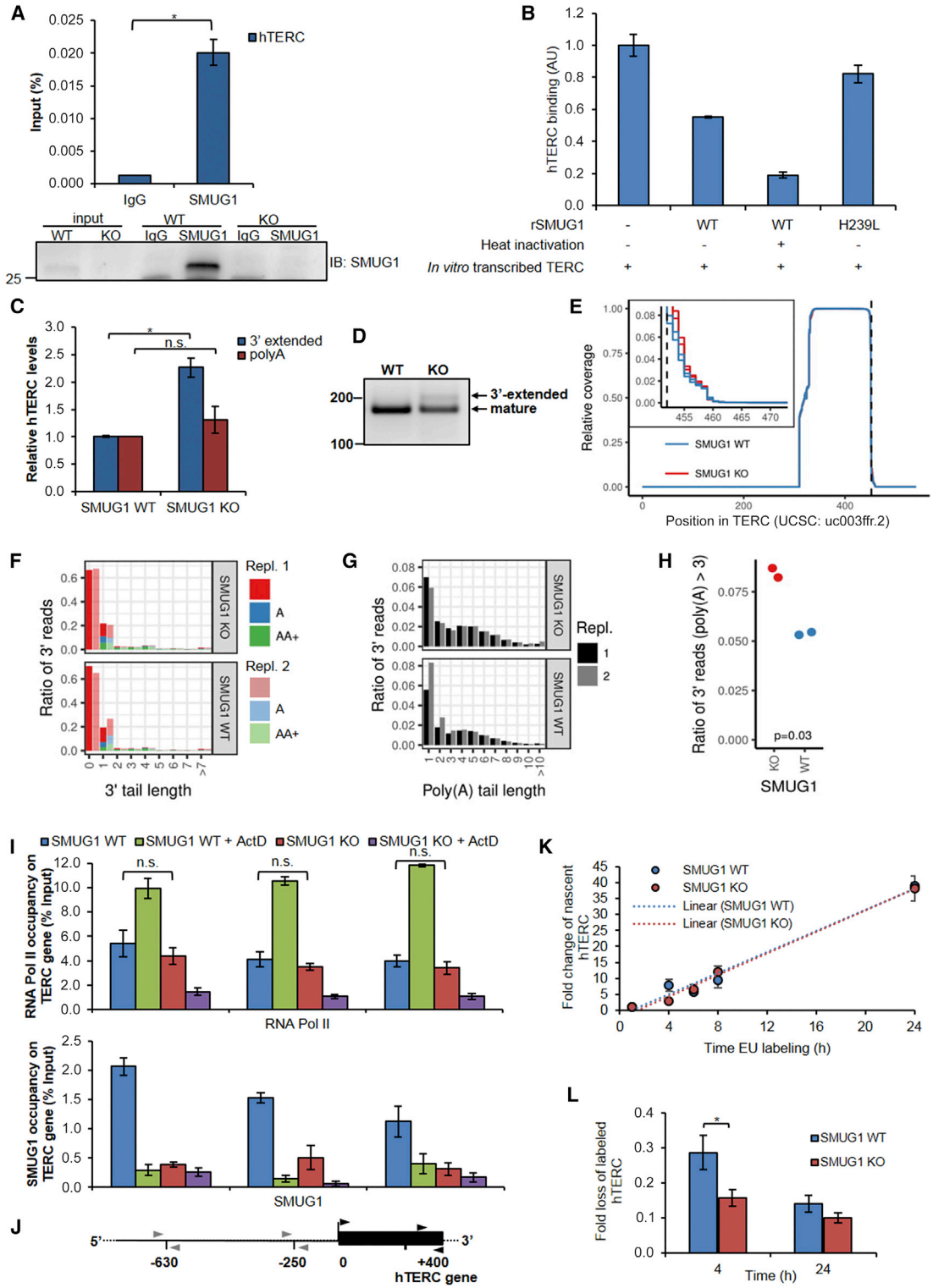


**Figure 5. SMUG1 Is Required for Co-transcriptional Processing of *hTERC***

(A) RNA immunoprecipitation (RIP) of *hTERC* by SMUG1 in HAP1 cells using an antibody against SMUG1, quantified by qPCR. Data are presented as percent of input RNA (top). Representative blot of immunoprecipitation for IgG and SMUG1 antibodies (bottom). IgG, negative control.

(B) *hTERC* binding by SMUG1 WT and H239L mutant measured via qPCR after His-tag pull-down using *in vitro* transcribed *hTERC* as prey.

(C) Levels of polyadenylated and 3′-extended *hTERC* relative to mature *hTERC* as quantified by qPCR.

*(legend continued on next page)*

SMUG1-KO cells compared to the WT (Figure 6A, right). No effect of pretreatment with APE1 alone was detectable (data not shown), suggesting that one or more modified bases that are substrates for SMUG1 are present in *hTERC* in human cells.

RNA-IP showed that DKC1 associated less efficiently with *hTERC* in SMUG1-KO cells (Figure 6B). Taken together, this suggests that the modified base(s) interfered with DKC1 binding. Since DKC1 stabilizes *hTERC* (Shukla et al., 2016; Venteicher et al., 2009; Vulliamy et al., 2008), this reduced association might contribute to the reduced *hTERC* stability in SMUG1-KO cells.

It is also possible that the *hTERC* species containing 3′-modified bases were degraded. Indeed, increased 3′-polyadenylation of *hTERC* was observed in SMUG1-KO cells (Figure 5C). If these species are degraded, inhibition of pathways involved in *hTERC* degradation should restore *hTERC* levels. As expected, small interfering RNA (siRNA)-mediated depletion of EXOSC10, the major RNA exosome, resulted in stabilization of *hTERC* in WT cells (Figures 6C, left; Figure S5). Although no difference in *hTERC* abundance could be detected in WT cells upon PARN depletion, the expected accumulation of polyadenylated *hTERC* was observed (Figure 6C, right). Simultaneous inhibition of the EXOSC10 and PARN enzymes did not result in any synergistic effects (Figure 6C), as expected, since these enzymes act in the same pathway (Shukla et al., 2016). Interestingly, stabilization of *hTERC* was not observed in SMUG1-KO cells upon *EXOSC10* silencing (Figure 6C).

We confirmed that DKC1 affects *hTERC* processing and stability (Shukla et al., 2016), as reduced *hTERC* was observed upon the depletion of DKC1 (Figure 6D, left). Interestingly, depletion of DKC1 in SMUG1-KO cells reduced *hTERC* levels further (Figure 6D). Depletion of PARN, either alone or together with DKC1, did not stabilize *hTERC* levels, but depletion of DKC1 together with EXOSC10 introduced a small stabilizing effect in both cell lines. High accumulation of polyadenylated *hTERC* upon DKC1 inhibition (96 h) was observed in SMUG1-KO cells (Figure 6D, right), consistent with the role of DKC1 in *hTERC* stabilization. No further accumulation of polyadenylated *hTERC* could be observed upon the silencing of *EXOSC10* or *PARN* in DKC1-depleted cells (Figure 6D, right). These results suggest that SMUG1 is required to funnel *hTERC* to the exosome machinery and that *hTERC* depletion occurs via an EXOSC10-independent pathway in SMUG1-KO cells.

In conclusion, SMUG1 is required for co-transcriptional processing of *hTERC* and functions in *hTERC* biogenesis by regulating the presence of base modifications that interfere with DKC1 binding. Consequently, loss of SMUG1 leads to an imbalance between mature *hTERC* and its processing intermediates, which are degraded in an EXOSC10-independent RNA degradation pathway (Figure 7).

## DISCUSSION

Here, we show that human SMUG1-DNA glycosylase is required for the maturation of *hTERC* through regulating the levels of modified bases in a region important for DKC1 binding. In the absence of SMUG1, *hTERC* molecules containing modified bases and processing intermediates accumulate, accompanied by reduced levels of mature *hTERC*. An insufficient *hTERC* level limits telomerase activity in SMUG1-KO cells, leading to severe telomere attrition.

SMUG1 is a multifunctional enzyme that acts both in BER (Nilsen et al., 2001) and in RNA processing (Jobert et al., 2013). To determine which activity is more important for telomere maintenance, we used a complementation strategy where we found that *hTERC* levels were limiting for telomerase activity in SMUG1-KO cells. Ectopic expression of SMUG1 restored *hTERC* levels and telomerase activity. As this was accompanied by increased telomere length, we conclude that the telomere maintenance defects are caused by loss of SMUG1. The SMUG1/DKC1 interaction appears essential for this function as a SMUG1 mutant that cannot bind DKC1 failed to restore telomere length. Some restoration of telomere length was seen after complementation with a SMUG1 nucleic acid binding mutant that, consequently, has low DNA-glycosylase activity on synthetic substrates *in vitro* (Matsubara et al., 2004). Because the ability to associate with DKC1 was preserved in this mutant (Jobert et al., 2013), the inability of the nucleic acid binding mutant to restore telomere length to the same extent as SMUG1 WT suggested that the DNA-glycosylase activity is also required.

A function for the DNA-glycosylase activity was further supported by the fact that binding of SMUG1 to *hTERC* appeared to require the presence of modified bases as we could only detect the association with *hTERC* isolated from cells and not *in vitro* transcribed *hTERC* that lacked modified bases. *hTERC* exhibited a greater number of modified bases in a region between the CR4/CR5 domain and the H box, where DKC1 binds. The nature of the modified base(s) in *hTERC* remains unknown as we were unable, despite some stabilization of *hTERC* after

(D) 3′-RACE products separated by agarose gel electrophoresis.
(E) Position-specific read profiles for 3′ RACE libraries. The graphs show the read depth for reads aligning to the *hTERC* gene locus, normalized to the maximum read depth within each library. The vertical dashed line shows the canonical *hTERC* 3′ end as described (Moon et al., 2015). The insert shows a zoom-in of the region immediately after the 3′ end.
(F) 3′-RACE products containing the canonical 3′ *hTERC* site (CAGGACTCGGCTCACACATGC). Reads containing the canonical 3′ *hTERC* site were classified based on the number of additional genome-matching nucleotides at their 3′ ends (x axis) and their 3′ poly(A) content (color). Cells were grouped by genotype; replicate samples are shown separately.
(G and H) Distribution (G) and ratio (H) of poly(A) tail length for 3′-RACE products containing the canonical 3′ *hTERC* site (CAGGACTCGGCTCACACATGC).
(I) Co-occupancy analysis of active RNA polymerase II (top) and SMUG1 (bottom) on the *hTERC* gene as measured by re-ChIP. ActD was used to inhibit RNA polymerase II.
(J) Schematic representation of the *hTERC* gene and its promoter region. The positions of the primers used (−630 through +400; +1 defined as the *hTERC* transcriptional start site) are indicated along the *hTERC* gene.
(K and L) Click-iT experiments showing nascent *hTERC* levels (K) and *hTERC* decay (L) over time in HAP1 cells.
(E–H) n = 2. (A–C, I, and L) Data represent means ±SEM, n = 3 *p ≤ 0.05, **p ≤ 0.01, and ****p ≤ 0.0001; ns, not significant (two-tailed Student's t test).

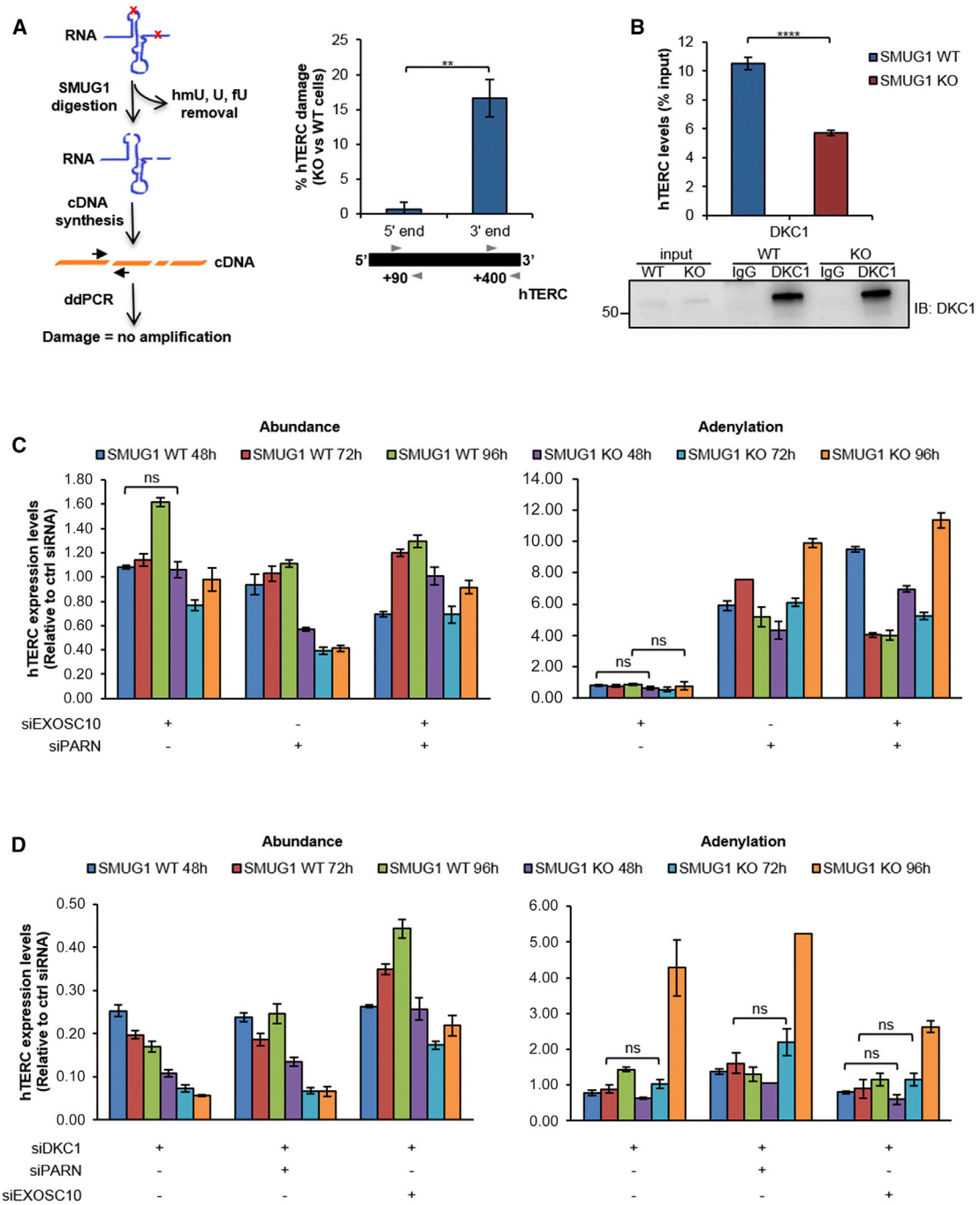


**Figure 6. The Absence of SMUG1 Affects *hTERC* Degradation**

(A) *hTERC* RNA damage levels at 5′ and 3′ regions as measured by ddPCR (right). RNA from HAP1 cells was digested with SMUG1 enzyme prior to cDNA synthesis (left). Primer positions are indicated along *hTERC*. An overview of the protocol is shown (left).

(B) qPCR showing *hTERC* immunoprecipitation by DKC1. Data are presented as percent of input RNA. Background signal given by IgG control was subtracted from the specific reaction (top). Representative blot of immunoprecipitation for IgG and DKC1 antibodies (bottom).

(C and D) Quantification of hTERC levels and adenylation frequency in HAP1 cells after siRNA-mediated depletion of EXOSC10 and PARN (C) or after DKC1, PARN, and EXOSC10 silencing (D) measured by qPCR. Cells were harvested at 48, 72, and 96 h after addition of siRNA. Relative abundance was measured using cDNA synthesized with random primers while adenylation frequency was estimated as the ratio of oligo(dT)-primed cDNA to random-primed cDNA.

(A–D) Data represent means ± SEM, ns, $^{**}p \leq 0.01$, $^{****}p \leq 0.0001$; ns, not significant (comparison between HAP1 SMUG1-WT and SMUG1-KO silenced for each time point, two-tailed Student's t test).

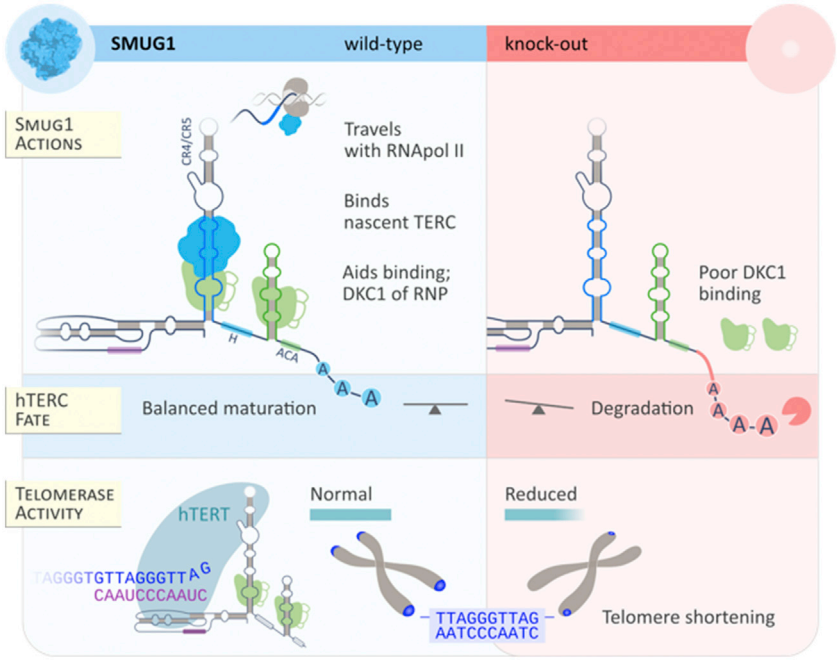


**Figure 7. Working Model**
Our data support a model where SMUG1 acts co-transcriptionally in *hTERC* biogenesis in a step upstream of the PARN/PABPN1 machinery by regulating the presence of modified bases in a region between CR4/CR5 and the H box. SMUG1 is required for efficient DKC1 binding and exosome-mediated degradation of these modified *hTERC* molecules. In SMUG1-KO cells the equilibrium between the mature *hTERC* and its processing intermediates is shifted toward degradation, leading to limiting amounts of *hTERC* unable to sustain telomerase activity. Figure by Ellen Tenstad/Science Shaped.

depletion of EXOSC10 and DKC1 (Figure 6D), to isolate sufficiently high amounts of *hTERC* from SMUG1-KO cells to perform lesion detection by LC-MS/MS. However, as treatment with APE1 alone did not reduce the amplification efficiency, we concluded that the base damage or modified bases accumulate in *hTERC* in SMUG1-KO are substrates for SMUG1. The likely substrate would be hmU or deoxyU, which we previously showed were substrates for SMUG1 in RNA (Jobert et al., 2013). Culturing cells in the presence of hmU did not, however, stimulate the association between SMUG1 and *hTERC* (Figure S3E). Thus, the association did not depend on exogenously induced modified RNA bases. The fact that we preferentially detected SMUG1 substrates toward the 3′ end of *hTERC*, as opposed to a uniform distribution, is more consistent with the presence of a base modification, rather than random damage. hmU has been identified in RNA (Jobert et al., 2013). Since it cannot be introduced into RNA by direct oxidation of thymine, it is likely formed by deamination of 5-hydroxymethylcytosine derived from 5-methylcytosine (Huber et al., 2015). It is tempting to speculate, therefore, that SMUG1 might regulate the presence of modified cytosines at two other methylated sites in *hTERC*, C323 and C455, which are located in the CR4/CR5 and the H box, respectively, the regions that accumulate base damage in SMUG1-KO cells.

Interestingly, the phenotype we observed in SMUG1-KO cells is reminiscent of that seen after depletion of HuR; HuR facilitated methylation of *hTERC* at C106, thereby promoting DKC1 binding to *hTERC* and assembly to hTERT (Tang et al., 2018). Our data present the possibility that SMUG1 might function as a dynamic regulator of DKC1 binding in response to base modifications in the CR4/CR5 domain, but further characterization of the specific bases requires the development of new mapping techniques. Whether dynamic modification of *hTERC* alters its secondary structure or otherwise interferes with DKC1 localization (Figure 1A) will be the focus of future studies.

*hTERC* levels could not be rescued by knocking down components of the RNA decay machinery. This suggests that SMUG1 is required to recruit the exosome and that other, yet-to-be-identified, degradation pathways may act in SMUG1-KO cells. Interestingly, SMUG1 stabilized the stalled RNA polymerase complex at the *hTERC* gene. The exosome is recruited co-transcriptionally, and Pol II backtracking provides a free RNA 3′ end for the core (Lemay et al., 2014). Our data do not suggest that SMUG1 affects *hTERC* transcriptional termination because long read-through molecules were not observed. The absence of large differences in the poly(A) distribution shows that the end-processing machinery is functional in SMUG1-KO cells. However, SMUG1-KO cells harbored higher levels of slightly elongated *hTERC* molecules, exhibiting base modification(s) toward their 3′ region. Hence, it is possible that SMUG1 acts co-transcriptionally to target *hTERC* containing hmU modified bases that interfere with DKC1 binding to the exosome.

Although the function of SMUG1 in *hTERC* biogenesis was the dominating phenotype in human SMUG1-KO cells, we did observe telomeric base damage (Figure 3F), which could contribute to the reduced binding of TRF2 and POT1 observed in TeloChIP experiments (Figure 3H), as the two main SMUG1 substrates (uracil [Vallabhaneni et al., 2015] and hmU [Theruvathu et al., 2014]) interfere with shelterin assembly *in vitro*. In addition, the short telomeres contain less available substrate for TRF1 and TRF2 binding, which might be the main reason for dys-localization of these proteins in SMUG1-KO cells (Figures 3G and S2B).

As observed previously in *Ogg1*$^{-/-}$ (Wang et al., 2010), *Nthl1*$^{-/-}$ (Vallabhaneni et al., 2013), and *Ung*$^{-/-}$ (Vallabhaneni et al., 2015) mice, *Smug1*$^{-/-}$ MEFs and mice show increased DNA damage in telomeres and multiple telomere defects (Figures 2 and S1D). In *Smug1*$^{-/-}$ mice, fragile telomeres and reduced proliferative capacity of bone marrow cells are seen in the presence of TERT, whereas in the other DNA-glycosylase-knockout mice, telomere maintenance defects become obvious first in the background of TERT deficiency (Vallabhaneni et al., 2015). It is possible that the function of SMUG1 in *Terc* biogenesis contributes to the apparently stronger telomere phenotype in *Smug1*$^{-/-}$ mice, but

although SMUG1 binds *Terc* in MEFs (Figure S1F), *Smug1*$^{-/-}$ MEFs did not show consistently reduced *Terc* levels (Figure S1G). Therefore, the telomere maintenance defects in MEFs appear to be mainly caused by the loss of SMUG1-dependent BER (Alsøe et al., 2017). Measurements of telomere fragility (Figures 2D, 2E, and S1D) indicated impaired replication of the C-rich telomere strand, which would be expected to contain more uracil lesions. However, as no method is available to discriminate between uracil and hmU in specific genomic regions, we do not know which SMUG1 substrate gives rise to these phenotypes in MEFs. Faithful BER of U has been shown to be needed to protect telomeres from unsolicited activation of mismatch repair at U:G pairs generated by activation-induced deaminase, leading to resection of the C-rich strand in *Ung*$^{-/-}$ B cells (Cortizas et al., 2016). We could not detect expression of AID in the HAP1 cells, but we cannot exclude the possibility that AID activation at one stage during establishment of the SMUG1-KO cell line is a cause of the extremely short telomeres in this cell line. In any case, the *hTERC* biogenesis defect prevented restoration of the telomeres.

Taken together, our data support a role of SMUG1 in telomere maintenance both as a BER enzyme and through its RNA processing function, but the extent to which these activities affect telomere maintenance differs between species and cell types. In human cells, SMUG1 acts in *hTERC* biogenesis by regulating the presence of modified bases in *hTERC* and facilitating DKC1 binding.

## STAR★METHODS

Detailed methods are provided in the online version of this paper and include the following:

- KEY RESOURCES TABLE
- LEAD CONTACT AND MATERIALS AVAILABILITY
- EXPERIMENTAL MODEL AND SUBJECT DETAILS
  - Animals
  - Cell Lines
- METHOD DETAILS
  - Cell Line Treatments
  - DNA and siRNA Transfections
  - Immunofluorescence
  - Proximity Ligation Assay (PLA)
  - Antibodies
  - Western Blot
  - hTERC *In Vitro* Transcription
  - Expression and Purification of SMUG1
  - His-tag and SMUG1 Pulldown
  - RNA Isolation and qPCR
  - EU Incorporation, Quantification of Nascent hTERC Kinetics, and hTERC Decay
  - RNA Sequencing and Analysis
  - hTERC RNA Damage Assay
  - Chromatin Immunoprecipitation (ChIP) and re-ChIP
  - Telomere ChIP
  - RNA Coimmunoprecipitation Assay
  - Northern Blot
  - 3′ RACE
  - 3′ RACE Library Preparation and Analysis
  - Bone Marrow Cell Isolation and Culture
  - Telomeric PNA FISH
  - Telomerase Activity
  - Telomere Length Analysis via qPCR
  - Telomeric DNA Damage Analysis
  - TRF Assay
- QUANTIFICATION AND STATISTICAL ANALYSIS
- DATA AND CODE AVAILABILITY

## SUPPLEMENTAL INFORMATION

Supplemental Information can be found online at https://doi.org/10.1016/j.celrep.2019.07.040.

## ACKNOWLEDGMENTS

We thank A.E. Moen, T. Tannæs, and T. Lüders for help and technical assistance and Primo Schär for sharing reagents. This work has been funded by grants to H.N. from the Research Council of Norway (grant no. 229633). L.L. was funded by a grant from the Norwegian Cancer Society (grant no. 4501723-2015). P.K. was funded by a PhD fellowship from the University of Oslo. L.A. was funded by a grant from the South East Regional Health Authority (project no. 274901). S.C. was funded by a grant from the Norwegian Cancer Society (grant no. 4501723-2013). P.Y. was funded by a grant from the South East Regional Health Authority (project no. 2017029). The research leading to these results has received funding from the European Union Seventh Framework Programme (FP7-PEOPLE-2013-COFUND) under grant agreement no. 609020 - Scientia Fellows to H.N. and A.G. BioCore is funded by the Faculty of Medicine at NTNU and Central Norway Regional Health Authority. P.S. is funded through grants from the Norwegian Research Council, Central Norway Regional Health Authority, and Stiftelsen Kristian Gerhard Jebsen. RNA sequencing was provided by the Genomics Core Facility (GCF), Norwegian University of Science and Technology (NTNU). GCF is funded by the Faculty of Medicine and Health Sciences at NTNU and the Central Norway Regional Health Authority. This work was initiated through a collaboration based on the COST action Cancer Control and Genomic Integrity (BM0703).

## AUTHOR CONTRIBUTIONS

P.K., L.L., S.C., A.G., Q.Y.E., L.J., L.A., and P.Y. performed experiments; P.K., L.L., P.S., S.G., and H.N. analyzed data; and P.K., L.L., and H.N. wrote the manuscript. All authors edited the manuscript.

## DECLARATION OF INTERESTS

The authors declare no competing interests.

Received: August 3, 2018
Revised: May 28, 2019
Accepted: July 14, 2019
Published: August 13, 2019

## REFERENCES

Aalbers, A.M., Kajigaya, S., van den Huevel-Eibrink, M.M., van der Velden, V.H., Calado, R.T., and Young, N.S. (2012). Human telomere disease due to disruption of the CCAAT box of the TERC promoter. Blood *119*, 3060–3063.

Alsøe, L., Sarno, A., Carracedo, S., Domanska, D., Dingler, F., Lirussi, L., Sen-Gupta, T., Tekin, N.B., Jobert, L., Alexandrov, L.B., et al. (2017). Uracil Accumulation and Mutagenesis Dominated by Cytosine Deamination in CpG Dinucleotides in Mice Lacking UNG and SMUG1. Sci. Rep. *7*, 7199.

Anders, S., Pyl, P.T., and Huber, W. (2015). HTSeq–a Python framework to work with high-throughput sequencing data. Bioinformatics *31*, 166–169.

Banfalvi, G. (2017). Overview of Cell Synchronization. Methods Mol. Biol. *1524*, 3–27.

Boyraz, B., Moon, D.H., Segal, M., Muosieyiri, M.Z., Aykanat, A., Tai, A.K., Cahan, P., and Agarwal, S. (2016). Posttranscriptional manipulation of TERC reverses molecular hallmarks of telomere disease. J. Clin. Invest. *126*, 3377–3382.

Cortizas, E.M., Zahn, A., Safavi, S., Reed, J.A., Vega, F., Di Noia, J.M., and Verdun, R.E. (2016). UNG protects B cells from AID-induced telomere loss. J. Exp. Med *213*, 2459–2472.

Dahl, J.A., and Collas, P. (2008). A rapid micro chromatin immunoprecipitation assay (microChIP). Nat. Protoc *3*, 1032–1045.

de Lange, T. (2005). Shelterin: the protein complex that shapes and safeguards human telomeres. Genes Dev *19*, 2100–2110.

Dobin, A., Davis, C.A., Schlesinger, F., Drenkow, J., Zaleski, C., Jha, S., Batut, P., Chaisson, M., and Gingeras, T.R. (2013). STAR: ultrafast universal RNA-seq aligner. Bioinformatics *29*, 15–21.

Egan, E.D., and Collins, K. (2012). An enhanced H/ACA RNP assembly mechanism for human telomerase RNA. Mol. Cell Biol *32*, 2428–2439.

Ge, J., Crosby, S.D., Heinz, M.E., Bessler, M., and Mason, P.J. (2010). SnoRNA microarray analysis reveals changes in H/ACA and C/D RNA levels caused by dyskerin ablation in mouse liver. Biochem. J *429*, 33–41.

Göhring, J., Fulcher, N., Jacak, J., and Riha, K. (2014). TeloTool: a new tool for telomere length measurement from terminal restriction fragment analysis with improved probe intensity correction. Nucleic Acids Res. *42*, e21.

Grolimund, L., Aeby, E., Hamelin, R., Armand, F., Chiappe, D., Moniatte, M., and Lingner, J. (2013). A quantitative telomeric cromatin isolation protocol identifies different telomeric states. Nat. Commun *4*, 2848.

Huber, S.M., van Delft, P., Mendil, L., Bachman, M., Smollett, K., Werner, F., Miska, E.A., and Balasubramanian, S. (2015). Formation and abundance of 5-hydroxymethylcytosine in RNA. ChemBioChem *16*, 752–755.

Jobert, L., Skjeldam, H.K., Dalhus, B., Galashevskaya, A., Vågbø, C.B., Bjørås, M., and Nilsen, H. (2013). The human base excision repair enzyme SMUG1 directly interacts with DKC1 and contributes to RNA quality control. Mol. Cell *49*, 339–345.

Langmead, B., and Salzberg, S.L. (2012). Fast gapped-read alignment with Bowtie 2. Nat. Methods *9*, 357–359.

Law, C.W., Chen, Y., Shi, W., and Smyth, G.K. (2014). voom: Precision weights unlock linear model analysis tools for RNA-seq read counts. Genome Biol. *15*, R29.

Lee, J.H., Lee, Y.S., Jeong, S.A., Khadka, P., Roth, J., and Chung, I.K. (2014). Catalytically active telomerase holoenzyme is assembled in the dense fibrillar component of the nucleolus during S phase. Histochem. Cell Biol. *141*, 137–152.

Lemay, J.F., Larochelle, M., Marguerat, S., Atkinson, S., Bähler, J., and Bachand, F. (2014). The RNA exosome promotes transcription termination of backtracked RNA polymerase II. Nat. Struct. Mol. Biol *21*, 916–926.

Ludlow, A.T., Robin, J.D., Sayed, M., Litterst, C.M., Shelton, D.N., Shay, J.W., and Wright, W.E. (2014). Quantitative telomerase enzyme activity determination using droplet digital PCR with single cell resolution. Nucleic Acids Res. *42*, e104.

MacNeil, D.E., Bensoussan, H.J., and Autexier, C. (2016). Telomerase Regulation from Beginning to the End. Genes (Basel) *7*, E64.

Matsubara, M., Tanaka, T., Terato, H., Ohmae, E., Izumi, S., Katayanagi, K., and Ide, H. (2004). Mutational analysis of the damage-recognition and catalytic mechanism of human SMUG1 DNA glycosylase. Nucleic Acids Res. *32*, 5291–5302.

Mitchell, J.R., Wood, E., and Collins, K. (1999). A telomerase component is defective in the human disease dyskeratosis congenital. Nature *402*, 551–555.

Moon, D.H., Segal, M., Boyraz, B., Guinan, E., Hofmann, I., Cahan, P., Tai, A.K., and Agarwal, S. (2015). Poly(A)-specific ribonuclease (PARN) mediates 3′-end maturation of the telomerase RNA component. Nat. Genet. *47*, 1482–1488.

Morin, G.B. (1989). The human telomere terminal transferase enzyme is a ribonucleoprotein that synthesizes TTAGGG repeats. Cell *59*, 521–529.

Nguyen, D., Grenier St-Sauveur, V., Bergeron, D., Dupuis-Sandoval, F., Scott, M.S., and Bachand, F. (2015). A Polyadenylation-Dependent 3′ End Maturation Pathway Is Required for the Synthesis of the Human Telomerase RNA. Cell Rep. *13*, 2244–2257.

Nilsen, H., Haushalter, K.A., Robins, P., Barnes, D.E., Verdine, G.L., and Lindahl, T. (2001). Excision of deaminated cytosine from the vertebrate genome: role of the SMUG1 uracil-DNA glycosylase. EMBO J. *20*, 4278–4286.

O'Callaghan, N.J., and Fenech, M. (2011). A quantitative PCR method for measuring absolute telomere length. Biol. Proced. Online *13*, 3.

Quinlan, A.R., and Hall, I.M. (2010). BEDTools: a flexible suite of utilities for comparing genomic features. Bioinformatics *26*, 841–842.

Ritchie, M.E., Phipson, B., Wu, D., Hu, Y., Law, C.W., Shi, W., and Smyth, G.K. (2015). limma powers differential expression analyses for RNA-sequencing and microarray studies. Nucleic Acids Res. *43*, e47.

Robinson, M.D., and Oshlack, A. (2010). A scaling normalization method for differential expression analysis of RNA-seq data. Genome Biol *11*, R25.

Schmidt, J.C., and Cech, T.R. (2015). Human telomerase: biogenesis, trafficking, recruitment, and activation. Genes Dev *29*, 1095–1105.

Shukla, S., Schmidt, J.C., Goldfarb, K.C., Cech, T.R., and Parker, R. (2016). Inhibition of telomerase RNA decay rescues telomerase deficiency caused by dyskerin or PARN defects. Nat. Struct. Mol. Biol *23*, 286–292.

Tang, H., Wang, H., Cheng, X., Fan, X., Yang, F., Zhang, M., Chen, Y., Tian, Y., Liu, C., Shao, D., et al. (2018). HuR regulates telomerase activity through TERC methylation. Nat. Commun. *9*, 2213.

Theruvathu, J.A., Darwanto, A., Hsu, C.W., and Sowers, L.C. (2014). The effect of Pot1 binding on the repair of thymine analogs in a telomeric DNA sequence. Nucleic Acids Res *42*, 9063–9073.

Tseng, C.K., Wang, H.F., Burns, A.M., Schroeder, M.R., Gaspari, M., and Baumann, P. (2015). Human Telomerase RNA Processing and Quality Control. Cell Rep. *13*, 2232–2243.

Vallabhaneni, H., O'Callaghan, N., Sidorova, J., and Liu, Y. (2013). Defective repair of oxidative base lesions by the DNA glycosylase Nth1 associates with multiple telomere defects. PLoS Genet *9*, e1003639.

Vallabhaneni, H., Zhou, F., Maul, R.W., Sarkar, J., Yin, J., Lei, M., Harrington, L., Gearhart, P.J., and Liu, Y. (2015). Defective repair of uracil causes telomere defects in mouse hematopoietic cells. J. Biol. Chem *290*, 5502–5511.

Venteicher, A.S., Abreu, E.B., Meng, Z., McCann, K.E., Terns, R.M., Veenstra, T.D., Terns, M.P., and Artandi, S.E. (2009). A human telomerase holoenzyme protein required for Cajal body localization and telomere synthesis. Science *323*, 644–648.

Vulliamy, T., Beswick, R., Kirwan, M., Marrone, A., Digweed, M., Walne, A., and Dokal, I. (2008). Mutations in the telomerase component NHP2 cause the premature ageing syndrome dyskeratosis congenital. Proc. Natl. Acad. Sci. USA *105*, 8073–8078.

Wang, Z., Rhee, D.B., Lu, J., Bohr, C.T., Zhou, F., Vallabhaneni, H., de Souza-Pinto, N.C., and Liu, Y. (2010). Characterization of oxidative guanine damage and repair in mammalian telomeres. PLoS Genet *6*, e1000951.

Xi, L., and Cech, T.R. (2014). Inventory of telomerase components in human cells reveals multiple subpopulations of hTR and hTERT. Nucleic Acids Res. *42*, 8565–8577.

Zhao, J.Q., Hoare, S.F., McFarlane, R., Muir, S., Parkinson, E.K., Black, D.M., and Keith, W.N. (1998). Cloning and characterization of human and mouse telomerase RNA gene promoter sequences. Oncogene *16*, 1345–1350.

Zimmermann, M., Kibe, T., Kabir, S., and de Lange, T. (2014). TRF1 negotiates TTAGGG repeat-associated replication problems by recruiting the BLM helicase and the TPP1/POT1 repressor of ATR signaling. Genes Dev. *28*, 2477–2491.

Zinder, J.C., and Lima, C.D. (2017). Targeting RNA for processing or destruction by the eukaryotic RNA exosome and its cofactors. Genes Dev *31*, 88–100.

## STAR★METHODS

### KEY RESOURCES TABLE

| REAGENT or RESOURCE | SOURCE | IDENTIFIER |
|---|---|---|
| Antibodies | | |
| Rabbit anti-SMUG1 | Abcam | Cat# ab192240 |
| Rabbit anti-IgG, Isotype control | Abcam | Cat# ab172730; RRID:AB_2687931 |
| Rabbit anti-RNA polymerase II CTD repeat YSPTSPS (phospho S5) | Abcam | Cat# ab5131; RRID:AB_449369 |
| Rabbit anti-His tag | Cell signaling technology | Cat# 2365; RRID:AB_2115720 |
| Rabbit anti-coilin | Cell signaling technology | Cat# 14168; RRID:AB_2798410 |
| Rabbit anti-DKC1 | Bethyl laboratories, Inc | Cat# A302-591A; RRID:AB_10554666 |
| Rat anti-BrdU | Abcam | Cat# ab6326; RRID:AB_305426 |
| Rabbit anti-TRF1 | Gift from DeLange lab | N/A |
| Rabbit anti-TRF2 | Gift from DeLange lab | N/A |
| Rabbit anti-HA tag (C29F4) | Cell signaling technology | Cat# 3724; RRID: AB_1549585 |
| Mouse anti-phospho Histone H2A.X (Ser139), clone JBW301 | Millipore | Cat# 05-636-2KL; RRID:AB_309864 |
| Rabbit anti-TRF2 | Novus Biologicals | Cat# NB110-57130; RRID:AB_844199 |
| Rabbit anti-POT1 | Abcam | Cat# ab21382; RRID:AB_777376 |
| Rabbit anti-POT1 | Abcam | Cat# ab240948 |
| Rabbit anti-Telomerase reverse transcriptase | Abcam | Cat# ab32020; RRID:AB_778296 |
| Rabbit anti-GAPDH | Cell signaling technology | Cat# 2118; RRID:AB_561053 |
| Monoclonal Anti-α-Tubulin antibody produced in mouse | Sigma-Aldrich-Aldrich | Cat# T5168; RRID:AB_477579 |
| Monoclonal ANTI-FLAG® M2 antibody produced in mouse | Sigma-Aldrich-Aldrich | Cat# F1804; RRID:AB_262044 |
| Rabbit anti-PARN | Abcam | Cat# ab188333 |
| Rabbit anti-EXOSC10 | Abcam | Cat# ab50558; RRID:AB_869937 |
| Goat anti-Mouse IgG (H+L) Secondary Antibody, HRP | Life Technologies | Cat# 31430; RRID:AB_228307 |
| Goat anti-Rabbit IgG (H+L) Secondary Antibody, HRP | Life Technologies | Cat# 31460; RRID:AB_228341 |
| Monoclonal Anti-Rabbit IgG, Native−Peroxidase antibody produced in mouse | Sigma-Aldrich-Aldrich | Cat# R3155; RRID:AB_1079117 |
| Goat anti-Rabbit IgG (H+L) Cross-Adsorbed Secondary Antibody, Alexa Fluor 594 | Life Technologies | Cat# A11012; RRID: AB_2534079 |
| Goat anti-Rat IgG (H+L) Cross-Adsorbed Secondary Antibody, Alexa Fluor 594 | Life Technologies | Cat# A11007; RRID: AB_10561522 |
| Goat anti-Rabbit IgG (H+L) Cross-Adsorbed ReadyProbes Secondary Antibody, Alexa Fluor 488 | Life Technologies | Cat# R37116; RRID: AB_2556544 |
| Goat anti-Mouse IgG (H+L) Cross-Adsorbed Secondary Antibody, Alexa Fluor 488 | Life Technologies | Cat# 11029; RRID: AB_2534088 |
| Bacterial and Virus Strains | | |
| *E. coli* BL21 (DE3) competent cells | Agilent technologies | Cat# 200131 |
| Biological Samples | | |
| Mouse: Bone marrow cells from Smug1$^{+/+}$ mice | Lab made | N/A |
| Mouse: Bone marrow cells from Smug1$^{-/-}$ mice | Lab made | N/A |
| Mouse: Liver tissue from Smug1$^{+/+}$ mice | Lab made | N/A |
| Mouse: Liver tissue from Smug1$^{-/-}$ mice | Lab made | N/A |
| Mouse: Spleen tissue from Smug1$^{+/+}$ mice | Lab made | N/A |

(*Continued on next page*)

*Continued*

| REAGENT or RESOURCE | SOURCE | IDENTIFIER |
|---|---|---|
| Mouse: Spleen tissue from Smug1$^{-/-}$ mice | Lab made | N/A |
| Chemicals, Peptides, and Recombinant Proteins | | |
| Phosphate buffered saline (PBS) | Lab made | N/A |
| Dulbecco's Modified Eagle Medium (DMEM) | Life Technologies | Cat# 10566016 |
| Iscove's Modified Dulbecco's Medium (IMDM) | Life Technologies | Cat# 31980048 |
| Dulbecco's Modified Eagle Medium/Nutrient Mixture F-12 (DMEM/F-12) | Life Technologies | Cat# 31331028 |
| Opti-MEM I Reduced Serum Medium | Life Technologies | Cat# 31985062 |
| Fetal Bovine Serum (FBS) | Sigma-Aldrich-Aldrich | Cat# F7524 |
| HyClone Calf Serum | Thermo Fisher | Cat# SH30073.03 |
| Penicillin-Streptomycin (10,000 U/mL) | Life Technologies | Cat# 15140122 |
| MEM Non-Essential Amino Acids Solution (100X) | Life Technologies | Cat# 11140035 |
| Lipofectamine 3000 Transfection Reagent | Life Technologies | Cat# L3000015 |
| Fugene 6 | Promega | Cat# E2691 |
| Lipofectamine RNAiMAX Transfection Reagent | Life Technologies | Cat# 13778150 |
| TRIzol Reagent | Life Technologies | Cat# 15596018 |
| Puromycin dihydrochloride | Sigma-Aldrich-Aldrich | Cat# P8833 |
| Actinomycin D | Sigma-Aldrich-Aldrich | Cat# A9415 |
| BrdU (5-Bromo-2'-Deoxyuridine) | Life Technologies | Cat# B23151 |
| Protease Inhibitor Cocktail | Sigma-Aldrich-Aldrich | Cat# P8340 |
| SMARTpool: siGENOME PARN siRNA | Dharmacon | Cat# M-011348-00-0005 |
| SMARTpool: siGENOME EXOSC10 siRNA | Dharmacon | Cat# M-010904-01-0005 |
| Silencer® Negative Control No. 1 siRNA | Ambion | Cat# AM4611 |
| Silencer DKC1 siRNA s4111 | Ambion | Cat# 4392420 |
| Silencer DKC1 siRNA s4112 | Ambion | Cat# 4457298 |
| ProLong Diamond Antifade Mountant with DAPI | Life Technologies | Cat# P36971 |
| Any kD Mini-PROTEAN® TGX Precast Protein Gels, 10-well, 50 μl | Bio-Rad | Cat# 456-9034 |
| SuperSignal West Femto Maximum Sensitivity Substrate | Life Technologies | Cat# 34095 |
| SuperSignal West Pico PLUS Chemiluminescent Substrate | Life Technologies | Cat# 34577 |
| RNeasy Mini Kit | QIAGEN | Cat# 74106 |
| iScript cDNA Synthesis Kit | Bio-Rad | Cat# 1708891 |
| iScript Select cDNA Synthesis Kit | Bio-Rad | Cat# 1708897 |
| Power SYBR Green PCR Master Mix | Life Technologies | Cat# 4367659 |
| *SIRV-Set 3 (Iso Mix E0 / ERCC)* | Lexogen | Cat# SKU: 051.01 |
| SuperScript IV Reverse Transcriptase | Life Technologies | Cat# 18090010 |
| hSMUG1 | New England Biolabs | Cat# M0336S |
| Dynabeads Protein G for Immunoprecipitation | Life Technologies | Cat# 10004D |
| QX200 ddPCR EvaGreen Supermix | Bio-Rad | Cat# 1864033 |
| Formaldehyde solution | Sigma-Aldrich-Aldrich | Cat# F8775 |
| DNase I, RNase-free (1 U/μL) | Life Technologies | Cat# EN0521 |
| DIG Easy Hyb Granules | Sigma-Aldrich-Aldrich | Cat# 11796895001 |
| Universal miRNA Cloning Linker | New England Biolabs | Cat# S1315S |
| T4 RNA Ligase 2, truncated KQ | New England Biolabs | Cat# M0373S |
| RNA Clean & Concentrator Kit | Zymo Research | Cat# R1013 |
| SuperScript III Reverse Transcriptase | Life Technologies | Cat# 18080093 |
| AccuPrime Pfx SuperMix | Life Technologies | Cat# 12344040 |

(*Continued on next page*)

*Continued*

| REAGENT or RESOURCE | SOURCE | IDENTIFIER |
|---|---|---|
| mouse IL-6 recombinant protein | eBioscience | Cat# 14-8061-80 |
| mouse stem cell factor (SCF) recombinant protein | eBioscience | Cat# 14-8341-63 |
| Mouse Methylcellulose Complete Media | R&D systems | Cat# HSC007 |
| Colcemid | Life Technologies | Cat# 15210040 |
| Blocking reagent | Sigma-Aldrich-Aldrich | Cat# 11096176001 |
| Vectashield mounting medium with DAPI | Vector labs | Cat# H-1200 |
| *Pierce BCA Protein Assay Kit* | Life Technologies | Cat# 23227 |
| *DNeasy Blood & Tissue Kit* | QIAGEN | Cat# 69504 |
| *APE1* | New England Biolabs | Cat# M0282S |
| Thymidine | Sigma-Aldrich-Aldrich | Cat# T1895 |
| Imidazole buffer Solution | Sigma-Aldrich-Aldrich | Cat# 68268 |
| Isopropyl β-D-1-thiogalactopyranoside | Sigma-Aldrich-Aldrich | Cat# I5502 |
| *Ni-NTA agarose resin* | QIAGEN | Cat# 30210 |
| *Econo-Column® Chromatography Columns* | Bio-Rad | Cat# 7372522 |
| *Bio-Scale Mini Macro-Prep High S cartridge* | Bio-Rad | Cat# 7324134 |
| *Ultrafree-MC Centrifugal Filter* | Millipore | Cat# UFC30DV0S |
| *HIS-Select® Nickel Magnetic Agarose beads* | Sigma-Aldrich-Aldrich | Cat# H9914 |
| SMUG1 wt recombinant protein | Lab made | N/A |
| SMUG1 H239L recombinant protein | Lab made | N/A |
| Critical Commercial Assays | | |
| SENSE Total RNA-Seq Library Prep Kit | Lexogen | Cat# SKU: 009.24 |
| Click-iT Nascent RNA Capture Kit, for gene expression analysis | Life Technologies | Cat# C10365 |
| DIG Oligonucleotide 3′ End Labeling Kit, 2nd generation | Sigma-Aldrich-Aldrich | Cat# 03353575910 |
| TeloTAGGG Telomere Length Assay | Sigma-Aldrich-Aldrich | Cat# 12209136001 |
| TruSeq Nano DNA Low Throughput Library Prep Kit | Illumina | Cat# 20015964 |
| MiSeq Reagent Kit v2 (500-cycles) | Illumina | Cat# MS-102-2003 |
| Duolink® *In Situ* Red Starter Kit Mouse/Rabbit | Sigma-Aldrich-Aldrich | Cat# DUO92101 |
| TRAPeze® Telomerase Detection Kit | Millipore | Cat# S7710 |
| MEGAscript T7 Transcription Kit | Life Technologies | Cat# AM1333 |
| Deposited Data | | |
| RNA-seq data | This study | GEO: GSE116580 |
| 3′ RACE seq data | This study | GEO: GSE116580 |
| Experimental Models: Cell Lines | | |
| Mouse: Mouse Embryonic fibroblasts *Smug1*$^{+/+}$ | Lab made | Alsøe et al., 2017 |
| Mouse: Mouse Embryonic fibroblasts *Smug1*$^{-/-}$ | Lab made | Alsøe et al., 2017 |
| Mouse: Mouse Embryonic fibroblasts *Smug1*$^{-/-}$_SMUG1 | Lab made | N/A |
| Mouse: Mouse Embryonic fibroblasts *Smug1*$^{-/-}$_H241L | Lab made | N/A |
| Mouse: Mouse Embryonic fibroblasts *Smug1*$^{-/-}$_E31R/E35R | Lab made | N/A |
| Human: HAP1 SMUG1-WT (control wild type cell line) | Horizon | Cat# HZGHC003300c009 |
| Human: HAP1 SMUG1-KO | Horizon | Cat# HZGHC003300c009 |
| Human: HAP1 SMUG1-KO_SMUG1 | Lab made | N/A |
| Human: HAP1 SMUG1-KO_SMUG1 H239L (NABm) | Lab made | N/A |
| Human: HAP1 SMUG1-KO_E29R/E33R/E231R (DBm) | Lab made | N/A |

(*Continued on next page*)

| Continued | | |
|---|---|---|
| REAGENT or RESOURCE | SOURCE | IDENTIFIER |
| Human: HeLa | ATCC | ATCC® CCL-2 |
| Experimental Models: Organisms/Strains | | |
| C56BL/6 Smug1$^{tm1Hln}$ (*Smug1*$^{-/-}$) | Lab made | Alsøe et al., 2017 |
| Oligonucleotides | | |
| See Table S1 for oligonucleotide information | | N/A |
| Recombinant DNA | | |
| Plasmid: pHH25-Smug1 | Cloned and stored in lab | N/A |
| Plasmid: pHH25-Smug1 H241L | Cloned and stored in lab | N/A |
| Plasmid: pHH25-Smug1 E31R/E35R | Cloned and stored in lab | N/A |
| Plasmid: pHH25-SMUG1 | Cloned and stored in lab | N/A |
| Plasmid: pHH25-SMUG1 H239L (NABm) | Cloned and stored in lab | N/A |
| Plasmid: pHH25-SMUG1 E29R/E31R/E231R (DBm) | Cloned and stored in lab | N/A |
| Plasmid: pCDNA-3xHA-hTERT | Addgene | Cat# 51631; RRID:Addgene_51637 |
| Plasmid: pBS U3-hTR-500 | Addgene | Cat# 28170; RRID:Addgene_28170 |
| Plasmid: pETM-11-hSMUG1 wt | Cloned and stored in lab | N/A |
| Plasmid: pETM-11-hSMUG1 H239L | Cloned and stored in lab | N/A |
| Software and Algorithms | | |
| Multi Gauge V3.1 software | Fujifilm | N/A |
| STAR aligner | Dobin et al., 2013 | https://github.com/alexdobin/STAR; RRID:SCR_015899 |
| htseq-count | Anders et al., 2015 | https://github.com/simon-anders/htseq; RRID:SCR_011867 |
| Voom | Law et al., 2014 | http://bioinf.wehi.edu.au/voom/ |
| Limma | Ritchie et al., 2015 | https://bioconductor.org/packages/release/bioc/html/limma.html; RRID:SCR_010943 |
| ImageJ | | https://imagej.net/Welcome; RRID:SCR_003070 |
| bowtie2 | Langmead and Salzberg, 2012 | http://bowtie-bio.sourceforge.net/bowtie2/index.shtml |
| Bedtools | Quinlan and Hall, 2010 | https://github.com/arq5x/bedtools2; RRID:SCR_006646 |
| TeloTool | Göhring et al., 2014 | https://github.com/jagoehring/TeloTool |
| Zeiss Zen blue and black | Zeiss | https://www.zeiss.com/microscopy/en_us/products/microscope-software/zen.html; RRID:SCR_013672 |
| GraphPad Prism | GraphPad | https://www.graphpad.com/; RRID:SCR_002798 |
| EZLogic Integration | Bio-Rad | http://www.bio-rad.com |

## LEAD CONTACT AND MATERIALS AVAILABILITY

Further information and request for reagents may be directed to and will be fulfilled by the Lead Contact, Hilde Nilsen (h.l.nilsen@medisin.uio.no).

Plasmids and human and mouse lines generated in this study are stored in the lab biobank and are available under request.

## EXPERIMENTAL MODEL AND SUBJECT DETAILS

### Animals

Wild-type and *Smug1*$^{-/-}$ C57BL/6J (male, 3- and 12-months old) mice were used for all the experiments. All mice were used straight after housing them until the appropriate experimental age. Animal maintenance, mouse handling and experimental procedures

were performed in accordance to institutional guidelines and procedures approved by the Animal Experimentation Administration in Norwegian Food Safety Authority (NFDA). The generation of *Smug1*$^{-/-}$ C57BL/6J mouse model was described previously (Alsøe et al., 2017).

### Cell Lines

Primary and transformed wild-type and *Smug1*$^{-/-}$ mouse embryonic fibroblasts (MEFs) were generated from the gene-targeted *Smug1*$^{-/-}$, *Smug1*$^{tm1Hln}$, C57BL/6J mouse model previously established in our lab (Alsøe et al., 2017). Timed matings were set up between either wild-type or *Smug1*$^{-/-}$ mice born from heterozygous parents in order to obtain wild-type and *Smug1*$^{-/-}$ embryos. Primary mouse embryonic fibroblasts (MEFs) were generated from ED13.5 to ED14.5 mouse tissue of wild-type and *Smug1*$^{-/-}$ embryos. Limbs were removed from embryos, the tissue was chopped into small pieces and cell suspension of all embryos deriving from one female was made using a pipette. Transformed wild-type and *Smug1*$^{-/-}$ MEFs were obtained by spontaneous transformation of the primary cultures. MEFs were grown in Dulbecco's Modified Eagle Medium/Nutrient Mixture F-12, GlutaMAX (Invitrogen) supplemented with 10% (vol/vol) fetal bovine serum (FBS, Lonza), 1x Penicillin-Streptomycin (Invitrogen) and 1x MEM non-essential amino acids (Invitrogen). Primary MEFs (Passage 1) and cells cultured for 22 continuous passages were used. The MEF genotypes were authenticated by PCR genotyping for Smug1$^{-/-}$ and SNPs for confirming C57BL/6J strain.

HAP1 cells were edited by CRISPR/Cas9 to contain a 2bp deletion in a coding exon of SMUG1. HAP1 SMUG1-WT and SMUG1-KO cells (Horizon) were maintained in culture as predominantly diploid cells in Iscove's modified Dulbecco's medium (IMDM, Life Technologies) containing 10% (vol/vol) FBS and 1x Penicillin/Streptomycin.

HeLa cells were purchased from ATCC and cultivated in Dulbecco's Modified Eagle Medium, GlutaMAX (Invitrogen) supplemented with 10% (vol/vol) fetal bovine serum (FBS, Lonza) and 1x Penicillin-Streptomycin (Invitrogen). HeLa cells were derived from female tissue while HAP1 cells were from a male cell line.

*Smug1*$^{-/-}$ MEF and HAP1 SMUG1-KO cells were complemented with different SMUG1 constructs cloned into the pHH25 vector. Transfection agents were FuGENE 6 (Promega) for MEF cells and Lipofectamine 3000 (Invitrogen) for HAP1 cells. Subsequently, stable cell lines re-expressing SMUG1 were selected using 2 μg/ml puromycin for MEFs and 1 μg/ml for HAP1 cells.

All the cell lines were cultured at 37°C and 5% $CO_2$.

## METHOD DETAILS

### Cell Line Treatments

HeLa cells transfected with Flag-tagged SMUG1 were synchronized at early S-phase by a double thymidine block (Banfalvi, 2017). Briefly, 24 h after seeding, cells were treated with 2 mM thymidine (Sigma-Aldrich) in complete medium for 14 h, washed twice in PBS and released in complete medium for 9 h. Then, cells were subjected to a second thymidine block (2 mM) for 14 h, washed twice in PBS and released in complete medium before fixation in PFA 4% at different time points.

To synchronize cells in S-phase, MEFs were seeded onto coverslips in a 24-well dish at 40% confluency. After 12 h, cells were serum starved for 42 h in DMEM supplemented with 0.5% FBS. Subsequently, cells were washed with 1x PBS and incubated in regular DMEM for another 24 h to re-enter the cell cycle. After 24 h, cells were given 1 h pulse with 20 μM bromodeoxyuridine (BrdU, BD Biosciences).

To inhibit RNA polymerase II, cells were treated for 2 h with 5 μg/ml of Actinomycin D (Sigma-Aldrich). For IR treatment, HAP1 cells were seeded onto coverslips in a 24-well cell culture dish and irradiated with 2 Gy. The next day, immunofluorescence experiments were conducted.

### DNA and siRNA Transfections

For overexpression and siRNA experiments, HAP1 cells were seeded onto 6-well plates or 10 cm dishes and transfected 24 h later. The constructs used for *hTERT* and *hTERC* overexpression were pCDNA-3xHA-hTERT and pBS-U3-hTR-500 (Addgene). For siRNA experiments, either a scrambled control siRNA or the target-specific siRNA was used. Lipofectamine 3000 and Lipofectamine RNAiMAX (Invitrogen) transfection reagents were used as per manufacturer's indications. The target-specific siRNAs for *PARN* and *EXOSC10* were purchased from Dharmacon as siGENOME SMARTpools; scrambled control and *DKC1* siRNAs were purchased from Ambion. Cells were harvested 24 h later and siRNA treated 48, 72 or 96 h after transfection.

### Immunofluorescence

Cells were seeded onto coverslips, fixed either in 70% ice cold ethanol for 10 min or with 4% paraformaldehyde at RT for 15 min and permeabilized with PBS containing 0.1% Triton X-100 at 4°C for 15 min. Cells were washed with 1x PBS and blocked for 1 h in PBS-BT solution (1x PBS, 3% BSA, 0.1% Triton X-100 and 0.05% sodium azide). Prior to blocking, antigen retrieval was necessary for BrdU labeling. Cells were incubated for 10 min on ice with 1 N HCl, 0.5% Triton X and 20 min 2 N HCl, 0.5% Triton X-100. Neutralization was followed, with 0.1 M sodium borate buffer pH 8.5. Cells were washed twice for 5 min in 1x PBS and incubated overnight at 4°C with primary antibodies in blocking solution. Cells were washed twice for 5 min in 1x PBS and secondary antibodies were added for 1 h (1:1000 dilution in PBS-BT). Cells were washed three times 5 min with 1x PBS. Coverslips were air-dried for 10 min, protected from light, and mounted onto ethanol rinsed glass slides using Prolong Diamond Antifade mounting medium containing DAPI and left

at room temperature overnight. Images were acquired using a Zeiss LSM780 confocal microscope with a 63x objective and analyzed using the Zeiss Zen Blue software.

### Proximity Ligation Assay (PLA)

Synchronized Flag-tagged SMUG1 cells fixed after 4 h of release were used for Figure 1C. After fixation with PFA 4% for 20 min at RT, cells were permeabilized for 5 min in PBS 0.25% (vol/vol) Triton X-100. Cells were incubated in blocking solution (FBS 10% in TBS 0.1% [vol/vol] Tween-20) for 1 h at RT. Incubation with primary antibodies (anti-Flag (Sigma-Aldrich) and RNAPII (Abcam) or anti-Coilin (Cell Signaling Technology) diluted 1:200 in blocking solution) was carried out ON at 4°C. After three washes in PLA Washing buffer A, PLA was performed following the manufacturer's protocol. Briefly, PLUS and MINUS PLA probes were diluted 1:5 in Duolink® Antibody diluent and added to the coverslips for 1 h at 37°C. Cells were washed twice in PLA Washing buffer A and the ligation step (ligase diluted 1:40 in Ligation buffer 1x) was carried out for 30 min at 37°C followed by amplification (Polymerase diluted 1:80 in Amplification buffer 1x) for 100 min at 37°C. Coverslips were washed twice in PLA Washing buffer B for 10 min each, in PLA Washing buffer A for 1 min and counterstained for Coilin/RNAPII, incubating the cells with Alexa Fluor 488 conjugated anti-rabbit (Life Technologies) for 2 h at RT. Cells were washed twice in PLA Washing buffer A for 2 min, rinsed with PLA Washing buffer B 0.01x and mounted with Prolong Diamond Antifade mounting medium. Technical control, represented by the omission of the anti-Flag antibody, resulted in loss of PLA signal.

### Antibodies

Primary antibodies used for immunofluorescence were DKC1 (1:500 and 1:50, Bethyl laboratories), BrdU (1:100, Abcam), Coilin (1:500, Cell Signaling Technology), Flag (1:200, Sigma-Aldrich), RNAPII (1:200, Abcam), TRF1 (1:500) and γH2Ax (1:500, Millipore). Secondary antibodies for immunofluorescence were purchased from Life Technologies: Alexa Fluor 594 conjugated goat-anti-rat/rabbit antibodies and Alexa Fluor 488 conjugated goat-anti-rabbit/mouse antibodies. Immunoblotting and ChIP/RIP experiments were carried out using the following antibodies: SMUG1 (1:2000 and 5 μg, Abcam), RNAPII (1:2000 and 5 mg, Abcam), PARN (1:2000, Abcam), EXOSC10 (1:2000, Abcam), HA (1:2000, Cell Signaling Technology), TRF2 (1:2000 and 5 μg, Novus Biologicals), POT1 (1:2000 and 5 μg, Abcam), DKC1 (5 μg, Bethyl Laboratories), TERT (1:2000, Abcam). Either GAPDH (1:3000, Cell Signaling Technology) or a-Tubulin (1:3000, Sigma-Aldrich) were used as loading controls.

### Western Blot

Whole-cell lysates were prepared in RIPA buffer [10 mM Tris-HCl (pH 8.0), 140 mM NaCl, 1 mM EDTA (pH 8.0), 0.5 mM EGTA, 0.1% SDS (wt/vol), 0.1% sodium deoxycholate (wt/vol) and 1% Triton X-100 (vol/vol)] containing protease inhibitors (Sigma-Aldrich). Protein extracts were run on any kD Mini-PROTEAN TGX precast gel (Bio-Rad) and blotted on nitrocellulose or PVDF membranes. Blots were blocked in either 5% non-fat milk or 5% BSA dissolved in 1x PBS, 0.1% Tween-20 (blocking solution). After the incubation with the specific primary antibody, secondary antibody incubation was carried out for 1 h (1:3000 in blocking solution) at RT. Blots were developed with SuperSignal West Pico or Femto Chemiluminescent substrate (Thermo Scientific). The signals were detected with a LAS-3000 mini imaging system (FujiFilm) and quantified with Multi Gauge V3.1 software.

### hTERC *In Vitro* Transcription

cDNA from HAP1 SMUG1-WT cells was used as a template to amplify *hTERC* for the *in vitro* transcription reaction. The primers used were: T7_hTERC_F, 5′-CCAAGCTTCTAATACGACTCACTATAGGGAGAGGGTTGCGGAGGGTGGGCCT-3′ and T7_hTERC_R, 5′-GCATGTGTGAGCCGAGTCCTGG-3′. PCR-amplified DNA was subsequently used as template to transcribe *hTERC* RNA *in vitro* by using the MEGAscript T7 transcription kit (Life Technologies), following the manufacturer's instructions.

### Expression and Purification of SMUG1

*E. coli* BL21(DE3) cells harboring pETM-11-hSMUG1 WT or H239L mutants were grown in LB media with kanamycin (50 μg/ml) at 37°C until $OD_{600}$ reached 0.6. The protein expression was induced with IPTG at 37°C for 2 h (final concentration 0.25 mM). The following procedures were performed at 4°C. Cells pelleted from 1 l culture were resuspended in 15 mL buffer A [50 mM Tris-HCl pH 8.0, 300 mM NaCl, 10 mM β-mercaptoethanol], disrupted by sonication (4 × 30 s at 60% amplitude), centrifuged (15000 rpm, 30 min), and incubated with 3 mL Ni-NTA agarose (QIAGEN) for 1 h with light agitation before loading onto an Econo-column (Bio-Rad; 2.5 × 20 cm). The column was washed with buffer A (50 ml); the fusion protein was eluted with buffer A containing 50 mM Imidazole (3 × 5 ml) and buffer A containing 150 mM Imidazole (3 × 5 ml). For hSMUG1 H239L, the eluted fractions were pooled and concentrated, glycerol was added (final concentration 25%) and stored at −20°C. For hSMUG1 WT, the eluted fractions were dialyzed against buffer B [20 mM MES pH 6.5, 50 mM NaCl, 10 mM β-mercaptoethanol] overnight. The fraction was centrifuged to remove the precipitate and concentrated to 10 ml, and loaded onto a Bio-Scale Mini Macro-Prep High S cartridge (Bio-Rad, 5 ml) onto the BioLogic DuoFlow 10 System (Bio-Rad). The column was washed with Buffer B and eluted with a linear gradient of NaCl (50-2000 mM) in buffer B. The fractions containing hSMUG1 were pooled and concentrated, glycerol was added (final concentration 25%) and stored at −20°C. In order to remove potential aggregated or degraded protein before His-tag and SMUG1 pulldown assays, diluted protein (1:10 in buffer A containing 10 mM Imidazole) was loaded onto 200 μL of pre-equilibrated Ni-NTA resin into Ultrafree-MC device (Sigma-Aldrich, 0.5 ml) and incubated for 30 min with light agitation. The resin was washed twice with buffer A containing 20 mM Imidazole (500 μl) and the protein eluted in 200 μL buffer A containing 250 mM Imidazole.

### His-tag and SMUG1 Pulldown

For the His-tag and SMUG1 pulldown experiments, 0.2 nmol of either full-length Hist-tag SMUG1 WT or SMUG1 H239L mutant was added, together with total RNA isolated from HAP1 SMUG1-WT cells (300 μg per reaction) or *in vitro* transcribed *hTERC* (5 μg per reaction) to 10 μL of HIS-Select® Nickel Magnetic Agarose beads (Sigma-Aldrich) or 20 μL Protein G magnetic beads (Life Technologies) conjugated with SMUG1 antibody (Abcam). As negative control, prior performing the assay, SMUG1 WT protein was heat inactivated at 65°C for 20 min. Binding was performed in PBS completed with protease inhibitor cocktail 1x (Sigma-Aldrich) for 3 h at 4°C under rotation. The beads were washed three times in washing buffer (PBS supplemented with 1% Igepal CA-630) and resuspended in Trizol (Invitrogen) or Laemmli sample buffer for RNA isolation and western blotting, respectively.

### RNA Isolation and qPCR

Total RNA was isolated with either RNeasy kit (QIAGEN) or with Trizol (Invitrogen) following the manufacturer's instructions. Reverse transcription was performed using the cDNA synthesis kits (Bio-Rad). Quantitative PCR was carried out on a QuantStudio 7 Flex detection system (Applied Biosystems) with Power SYBR green PCR master mix (Applied Biosystems). Each sample was analyzed in triplicate.

### EU Incorporation, Quantification of Nascent hTERC Kinetics, and hTERC Decay

Detection of nascent *hTERC* and its decay were analyzed by using the Click-iT® Nascent RNA Capture kit (Life Technologies). 5-ethynyl Uridine (EU) (Life Technologies) was dissolved in DMSO at a concentration of 200 mM. HAP1 cells were incubated with 0.2 mM EU for different time points (1, 4, 8 and 24 h) for capturing the nascent *hTERC* or pulsed for two hours and chased for 4 and 24 h for analyzing the *hTERC* decay. Cell pellets were harvested and total RNA prepared using Trizol reagent (Invitrogen). The biotinylation, the streptavidin binding and cDNA synthesis were performed as per manufacturer's instructions. qPCR analysis was performed using the standard protocol.

### RNA Sequencing and Analysis

RNA integrity was verified using the 2100 Bioanalyzer instrument. RNAs, spiked with control RNAs (Lexogen SIRV-Set 3) during cell lysis prior to RNA isolation, were submitted to the Genomic Core Facility (NTNU) for library preparation (Lexogen SENSE Total RNA-Seq Library Prep Kit) and sequencing (76 nucleotide paired end sequencing on an Illumina NextSeq 500 High Output flow cell). Sequence reads were aligned to the human genome (version GRCh38.p7) and to the control RNA sequences with the STAR aligner (Dobin et al., 2013). Read counts per gene (Encode release 84) were determined with htseq-count (Anders et al., 2015). The gene count matrix was normalized with voom (Law et al., 2014), using normalization factors computed with the TMM method (Robinson and Oshlack, 2010) from the reads aligning to the control RNAs. The normalized matrix was analyzed for differential gene expression with limma (Ritchie et al., 2015). Data is deposited in GEO: GSE116580.

### hTERC RNA Damage Assay

RNA isolated from HAP1 cells was digested with 2 U of SMUG1 (New England Biolabs) at 37°C for 30 min and then retro-transcribed with SuperScript IV RT (Invitrogen) following the manufacturer's instructions. Then, the cDNA was assayed via ddPCR using Droplet Digital PCR QX system (Bio-Rad). Briefly, the cDNA was added to a 20 μL PCR mixture containing 10 μL 2x QX200 ddPCR EvaGreen Supermix (Bio-Rad) and 100 nM *hTERC* specific primers. 20 μL of PCR mixture and 70 μL Droplet generation oil for EvaGreen (Bio-Rad) were mixed. Droplets were generated using a QX100 Droplet Generator (Bio-Rad). The following PCR conditions were used: after denaturing at 95°C for 5 min, 40 cycles at 95°C for 30 s and 60°C for 1 min were followed by 1 step at 4°C for 5 min and 90°C for 5 min. Reactions were read in the QX200 Droplet Reader (Bio-Rad).

### Chromatin Immunoprecipitation (ChIP) and re-ChIP

Chromatin immunoprecipitation was performed essentially as described by Dahl and Collas (2008). For re-ChIP experiments, the elution for the first immunoprecipitation (RNA polymerase II antibody) was performed in TE-SDS 0.5%, 10 mM DTT for 30 min at 37°C. 10% of the eluted chromatin was then retained as the primary ChIP. The remaining 90% was diluted 20 times in RIPA buffer (Dahl and Collas, 2008) and incubated overnight at 4°C with SMUG1 or IgG (isotype control) antibodies. Immunoprecipitates were then processed as described (Dahl and Collas, 2008). The purified DNA was analyzed via qPCR. Fold enrichment as percent of input was calculated by normalizing ChIP reactions to input DNA of the target gene.

### Telomere ChIP

Telomere ChIP (TeloChIP) analysis was carried out essentially as described previously (Grolimund et al., 2013). Briefly, cells were washed twice in PBS and cross-linked in 1% formaldehyde-1x PBS for 10 min at room temperature. Glycine (pH 2.5) was added to 125 mM in order to quench the reaction before washing the cells twice with PBS. Cells were lysed in lysis buffer [1% SDS, 10 mM EDTA (pH 8.0), 50 mM Tris-HCl (pH 8.0), EDTA-free protease inhibitor complex] and incubated for 5 min at room temperature, centrifuged for 5 min at 1,500 x*g*, washed once in lysis buffer and centrifuged as above. The chromatin-enriched pellets were resuspended in lysis buffer and sonicated for 25 cycles with 30 s ON and 30 s OFF per cycle using a Bioruptor (Diagenode). The sonicated lysate was centrifuged at 4°C for 15 min at 20,000 x*g*. The supernatant was diluted in 2 volumes of ChIP dilution buffer [0.75% Triton

X-100, 10 mM EDTA (pH 8.0), 50 mM Tris-HCl (pH 8.0), 600 mM NaCl]. The lysate was incubated with POT1, TRF2, SMUG1 antibodies or normal rabbit IgG covalently coupled to Protein G dynabeads (Invitrogen). The ChIP was performed at 4°C overnight. Beads were washed once with wash buffer 1 [0.1% SDS (wt/vol), 1% Triton X-100 (vol/vol), 2 mM EDTA (pH 8.0), 20 mM Tris-HCl (pH 8.0), 300 mM NaCl], wash buffer 2 [0.1% SDS (wt/vol), 1% Triton X-100 (vol/vol), 2 mM EDTA (pH 8.0), 20 mM Tris-HCl (pH 8.0), 500 mM NaCl], wash buffer 3 [500 mM LiCl, 1% NP-40 (vol/vol), 1% Na-deoxycholate (wt/vol), 1 mM EDTA (pH 8.0), 10 mM Tris-HCl (pH 8.0)] and twice with wash buffer 4 [1 mM EDTA (pH 8.0), 10 mM Tris-HCl (pH 8.0)]. DNA–protein complexes were eluted with 2.5 bead volumes of Elution buffer [20 mM Tris–HCl (pH 7.5), 5 mM EDTA (ph 8.0), 50 mM NaCl, 20 mM Na-butyrate, 1% SDS (wt/vol), 50 μg/ml proteinase K]. DNA-protein complexes were incubated for 2 h at 68°C, 1,300 xg. The DNA was extracted with phenol–chloroform–isoamylalcohol procedure and telomeric DNA sequences were analyzed using qPCR. Data are analyzed as percentage of input for each target gene. The primer sequences were previously described (O'Callaghan and Fenech, 2011).

### RNA Coimmunoprecipitation Assay

RNA immunoprecipitation assay was performed as described previously (Jobert et al., 2013) with minor modifications. Briefly, cells were washed twice in PBS and cross-linked in 1% formaldehyde-1x PBS for 10 min at room temperature. Glycine (pH 2.5) was added to 0.2 M in order to quench the reaction before washing the cells twice with ice-cold PBS. Cells were lysed in lysis buffer A [50 mM HEPES (pH 7.8), 1 mM EDTA (pH 8.0), 1% Triton X-100 (vol/vol), EDTA-free protease inhibitor complex] and sonicated for 10 cycles with 30 s ON and 30 s OFF per cycle using a Bioruptor (Diagenode). The sonicated lysate was diluted in 1 volume of lysis buffer B [50 mM HEPES (pH 7.8), 1 mM EDTA (pH 8.0), 50 mM $MgCl_2$, 10 mM $CaCl_2$, 0.4 U/μl RNaseOUT recombinant ribonuclease inhibitor (Invitrogen)]. DNA was digested with DNase I RNase free (Life Technologies) at 37°C for 15 min and digestion was stopped adding 20 mM EDTA (pH 8.0). The lysate was centrifuged at 4°C for 5 min at 20,000 x*g*. The supernatant was incubated with SMUG1, DKC1 or normal rabbit IgG covalently coupled to Protein G dynabeads (Invitrogen). The RIP was performed at 4°C overnight. Beads were washed once with Binding buffer [50 mM HEPES (pH 7.8), 20 mM EDTA (pH 8.0), 0.5% Triton X-100 (vol/vol), 25 mM $MgCl_2$, 5 mM $CaCl_2$], FA500 buffer [50 mM HEPES (pH 7.8), 1 mM EDTA (pH 8.0), 1% Triton X-100 (vol/vol), 500 mM NaCl, 0.1% Na-deoxycholate (wt/vol)], LiCl buffer [10 mM Tris-HCl (pH 7.5), 1% Triton X-100 (vol/vol), 1 mM EDTA (pH 8.0), 250 mM LiCl, 0.5% Na-deoxycholate (wt/vol)] and TES buffer [10 mM Tris-HCl (pH 7.5), 1 mM EDTA (pH 8.0), 10 mM NaCl]. RNA–protein complexes were eluted twice with 2.5 bead volumes of Elution buffer [100 mM Tris-HCl (pH 7.8), 10 mM EDTA (pH 8.0), 1% SDS (wt/vol)] for 10 min at 37°C. RNA-protein complexes and input samples were reverse-crosslinked with 200 mM NaCl for 1 h at 65°C and incubated at 42°C for 1 h after adding 20 μg proteinase K. The RNA was extracted with Trizol solution (Invitrogen) and analyzed by qPCR as percentage of input.

### Northern Blot

Oligonucleotide probes were labeled using the DIG Oligonucleotide 3′ End Labeling Kit, 2nd generation (Roche) following the manufacturer's instructions.

Northern blot analyses were carried out as described previously (Xi and Cech, 2014). Briefly, 5 μg of RNA samples were mixed with equal volume of 2x formamide loading dye, heated at 95°C for 5 min and then run on a 8% polyacrylamide/7 M urea/1x TBE at 60 V for 1 h. Membranes were cross-linked at 365 nm for 20 min in a UV crosslinker (Stratalinker). The membrane was pre-hybridized in DIG Easy Hyb Granules (Roche) at 42°C for 1 h and then hybridized in DIG Easy Hyb Granules with 3′ end DIG labeled oligo probes at 42°C overnight. The membrane was washed twice in prewarmed stringent wash buffer I (2x SSC, 0.1% SDS (wt/vol)) and stringent wash buffer II (0.2x SSC, 0.1% SDS (wt/vol)) at 50°C. After that, the membrane was blocked for 1 h at room temperature with 1x blocking solution (Roche) (1x blocking solution, 1x maleic acid buffer) and then incubated for 2 h with anti-DIG-AP antibody diluted in 1x blocking solution. The membrane was washed twice in 1x washing solution (Roche) for 15 min and then incubated with the 1x detection buffer (Roche) for 2 min and the substrate solution (CDP Star, Roche) for 5 min. Signals were detected with a LAS-3000 mini imaging system (FujiFilm) and quantified with ImageJ software. Probes for *hTERC* and *H1* were previously described (Boyraz et al., 2016; Moon et al., 2015; Nguyen et al., 2015).

### 3′ RACE

3′ RACE experiments were carried out as described previously (Moon et al., 2015). Briefly, 600 ng of total RNA were added in a 20-μl reaction containing 5 μM of Universal miRNA Cloning Linker (New England Biolabs), 280 U of T4 RNA ligase, Truncated KQ (NEW ENGLAND BIOLABS), 25% PEG8000 and 1 μl of RNaseOUT (Life Technologies) and incubated at 25°C for 16 h. RNA was cleaned using RNA Clean and Concentrator columns (Zymo Research), digested with DNase I (Life Technologies) at RT for 15 min and retro-transcribed with 5 pmol of Universal RT primer (5′-CTACGTAACGATTGATGGTGCCTACAG-3′) using SuperScript III RT (Invitrogen). PCR amplification was performed with 5 μM of TERC_L2 and universal RT primer set using AccuPrime Pfx SuperMix (Invitrogen) following the manufacturer's instructions. PCR reactions were separated onto 2.5% agarose gel.

### 3′ RACE Library Preparation and Analysis

3′ RACE products were prepared for sequencing using the TruSeq Nano DNA LT Library Prep kit (Illumina), following the manufacturer's instructions. The pooled completed libraries were sequenced on an Illumina MiSeq instrument with paired-end 250-base reads using the Illumina TruSeq v2 500 Cycles kit. For data analysis, paired end reads were aligned to the *hTERC* gene sequence (UCSC gene ID uc003ffr.2) by running bowtie2 (Langmead and Salzberg, 2012) in local alignment mode. Read pairs aligning to

the *hTERC* gene were further filtered by requiring that the reads mapped to opposite strands of the *hTERC* gene and that the reads represented plausible *hTERC* RNA fragments instead of primer artifacts. Specifically, we only kept read pairs where the estimated template lengths (unsigned value of SAM field 9) was identical and > 0, and where the signed template length (SAM field 9) had opposite signs for the read pair. We used the bedtools software (Quinlan and Hall, 2010) to compute read coverage. For the poly(A) analyses, we further filtered the *hTERC*-aligning reads by only keeping the rightmost-aligning read of each read pair that also contained the sequence corresponding to the canonical *hTERC* 3′ end (CAGGACTCGGCTCACACATGC). For each such read, we removed the 3′ adaptor sequence (by using cutadapt) and the 5′ part of the read that matched the *hTERC* gene sequence (up to 8 nucleotides downstream of the canonical *hTERC* 3′ end), and only kept those with at least one adenine and at most 25% other nucleotides within the remaining sequence. The length of these remaining sequences was the estimated poly(A) tail lengths.

### Bone Marrow Cell Isolation and Culture

Femurs and tibias were isolated and muscles were removed before the bones were rinsed with 70% ethanol and ice-cold HBSS under sterile conditions. For each bone, and upon separation of femurs from tibias, epiphyses were cut and bone marrow cells were flushed with 10 mL HBSS with a 26-gauge needle and passed through a 100 μm cell strainer (Corning). The inner surface of each bone was scraped with a needle. Cells were then spun at 300 x*g* for 15 min. Cell pellets were resuspended with 5 mL 1x RBC lysis buffer (eBioscience) and incubated at RT for 4 min. Lysis was stopped by adding 25 mL of ice-cold HBSS. Cells were then spun at 400 x*g* for 15 min at 4°C, resuspended in 10 mL of ice-cold HBSS and passed through a 30 μm pre-separation filter (Miltenyi Biotec). Upon cell counting, cells were spun at 300 x*g* for 15 min at 4°C and resuspended at 0.5 × $10^6$ cells/ml in IMDM (GIBCO) supplemented with 20% fetal calf serum (Hyclone, Logan, UT) in the presence of interleukin 6 (200 ng/ml, Affymetrix eBioscience) and stem cell factor (100 ng/ml; Affymetrix eBioscience). Cells were split every two days until passage 3.

Bone marrow cell (BMC) colony formation assay was performed by using methylcellulose-based media (R&D systems) according to the manufacturer's instructions. Twentyfive thousand BMCs were seeded in triplicates for each BMC isolation at day 0, and colonies were counted at day 11. Three different mice per genotype and generation were used.

### Telomeric PNA FISH

Cells were treated with 0.1 μg/ml Colcemid for 3 h prior to harvest and centrifuged at 300 x*g* for 5 min. Pellets were carefully resuspended in 7 mL of prewarmed 75 mM KCl. Tubes were placed in a 37°C water bath for 15 min and immediately centrifuged at 120 x*g* for 5 min. Pellets were resuspended in 2 mL of freshly prepared methanol:glacial acetic acid (3:1) fixative. To obtain metaphases, fixed cells were dropped onto slides and dried. Fluorescent *in situ* hybridization (FISH) was performed as earlier described (Zimmermann et al., 2014) with minor modifications. Briefly, slides were rehydrated in PBS (pH 7.0-7.5) for 5 min, fixed in 4% formaldehyde in PBS for 2 min, washed in PBS 3 × 5 min, treated at 37°C with freshly made 1 mg/ml pepsin in 10 mM glycine (pH 2), washed twice in PBS for 2 min, and dehydrated for 5 min in increasing concentrations of ethanol (70%, 95%, and 100%). After air-drying, 10 μL hybridization mix (10 mM Tris-HCl pH 7.2, 70% formamide, 0.5% blocking reagent (Roche) and probes (TelG-TAMRA or FITC-TelC, Biosynthesis) were applied. After addition of coverslips, the slides were heated on a 80°C hot plate for 3 min. Metaphases were hybridized for 2 h at RT in the dark in a humid chamber, washed two times 15 min with washing solution #1 (10 mM Tris-HCl pH 7.2, 70% formamide, 0.1% BSA), three times 5 min with washing solution #2 (0.1 M Tris-HCl pH 7.2, 0.15 M NaCl, 0.08% Tween-20), and dehydrated as described above. Slides were air-dried for 15 min and mounted with DAPI-containing mounting medium (VectaShield).

### Telomerase Activity

Telomerase activity was conducted either by using the qPCR or the ddPCR method. Cells were lysed in CHAPS buffer (TRAPeze kit, Millipore) for 30 min on ice. Protein determination of lysates was conducted using a BCA method. qPCR method was performed using the TRAPeze kit according to manufacturer's instructions. The protein amount used was 500 ng. The ddPCR method was used as previously described (Ludlow et al., 2014). Briefly, 10 μL of lysate, with concentrations 30-90 ng/μL, was added to a 50 μL extension reaction containing 1x TRAP reaction buffer (10x concentration: 200 mM Tris-HCl, pH 8.3, 15 mM $MgCl_2$), 0.4 mg/ml BSA, TS telomerase extension substrate (HPLC purified, 200 nM, dNTPs (2.5 mM each) and incubated for 40 min at 25°C then held at 4°C. The ddPCR reaction was assembled containing 1x EvaGreen ddPCR Supermix v2.0 (Bio-Rad), 50 nM TS primer, 50 nM ACX primer, 10 μL of extension product on a final volume of 25 μL. The lysis-extension mixture was subsequently used for the standard ddTRAP protocol. Droplets were generated according to the manufacturer's instructions and transferred to a 96-well PCR plate. The PCR program used was 95°C for 5 min, followed by 40 cycles of 95°C for 30 s, 54°C for 30 s, 72°C for 30 s, then held at 12°C. Following PCR, the fluorescence was read on the droplet reader using the 6-Fam channel.

### Telomere Length Analysis via qPCR

Genomic DNA (gDNA) was extracted from cells and tissues using the DNeasy Blood & Tissue Kit (QIAGEN). Average telomere length was measured from total gDNA samples by using the qPCR method (Anders et al., 2015) with minor modifications. The single-copy genes β-globin and 36B4 were used as references for human and mouse material, respectively. Each reaction included 5 μL 2x Power SYBR Green PCR Master mix (Applied Biosystems), 0.1 μL 10 μM telo forward and 0.9 μL 10 μM telo reverse primers, 2 μL water and 2 μL gDNA (5 ng/μL for human and 0.5 ng/μL for mouse) to yield a 10-μL reaction. Each single copy gene reaction included 5 μL 2x Power SYBR Green PCR Master mix (Applied Biosystems), 0.3 μL of 10 μM single copy gene forward and 0.7 μL 10 μM single copy

gene reverse primers, 2 μL water and 2 μL gDNA (5 ng/μL) to yield a 10-μL reaction. A QuantStudio 7 Flex Real-Time PCR System (Applied Biosystems) was used with reaction conditions of 95°C for 10 min followed by 40 cycles of data collection at 95°C for 15 s, 60°C anneal for 30 s, and 72°C extend for 45 s.

### Telomeric DNA Damage Analysis

gDNA (200 ng) isolated from mice tissues was digested with 10 U of SMUG1 (New England Biolabs) in a final concentration of 10 μL, at 37°C for 30 min. 5 μL of the reaction were further digested with 10 U of APE1 (New England Biolabs), at 37°C for 30 min. The standard protocol for telomere length analysis via qPCR was then conducted, using 1.5 ng of digested gDNA. Results were normalized to the uncut gDNA qPCR reaction.

### TRF Assay

Absolute telomere length analysis was carried out using the TeloTAGGG telomere length assay (Roche) according to the manufacturer's instructions with minor modifications. Briefly, 5 −10 μg of gDNA were digested with RsaI (20 U/reaction) and HinfI (20 U/reaction) restriction enzymes on a final volume of 20 μL, leaving the telomeric and subtelomeric sequence unaffected. In order to evaluate the presence of SMUG1 substrates in telomeric DNA, SMUG1 (5 U/reaction) and APE1 (1 U/reaction) enzymes (New England Biolabs) were added together with RsaI (10 U/reaction) and HinfI (10 U/reaction) on a final volume of 20 μL, using the SmartCut (New England Biolabs) digestion buffer. The digested gDNA was separated using a 0.8% standard gel electrophoresis, transferred via a semi-dry method to a Hybond XL (GE Healthcare) membrane, and hybridized using a DIG-labeled $(TTAGGG)_3$ oligonucleotide probe. Images were acquired on LAS-3000 mini imaging system (FujiFilm), and quantification was performed using the TeloTool software.

## QUANTIFICATION AND STATISTICAL ANALYSIS

All quantified data are presented as mean ± s.e.m., mean ± s.d. and fold change unless stated otherwise (refer to figure legend to detailed information). Student t test or one-way ANOVA were used to assess statistical significance in GraphPad Prism 7 (GraphPad software). A $p < 0.05$ was considered as statistical significant. P values were indicated with asterisks. Replicates, statistical tests carried out and statistical significances are reported in the corresponding figure legends.

## DATA AND CODE AVAILABILITY

Raw and analyzed RNA-seq and 3′ RACE-seq data have been deposited in the NCBI GEO database under accession number GEO: GSE116580.